

GHOST: Using Only Host Galaxy Information to Accurately Associate and Distinguish Supernovae

ALEX GAGLIANO,^{1,2,3,4} GAUTHAM NARAYAN,^{1,2,3} ANDREW ENGEL¹ AND MATIAS CARRASCO KIND^{1,2,3}

(THE DARK ENERGY SCIENCE COLLABORATION)

¹*Department of Astronomy, University of Illinois at Urbana-Champaign, Urbana, IL 61801, USA*

²*National Center for Supercomputing Applications, Urbana, IL 61801, USA*

³*Center for Astrophysical Surveys, Urbana, IL, 61801, USA*

⁴*NSF Graduate Research Fellow*

ABSTRACT

We present **GHOST**, a database of 16,175 spectroscopically classified supernovae and the properties of their host galaxies. We have developed a host galaxy association method using image gradients that achieves fewer misassociations for low- z hosts and higher completeness for high- z hosts than previous methods. We use dimensionality reduction to identify the host galaxy properties that distinguish supernova classes. Our results suggest that the hosts of SLSNe, SNe Ia, and core collapse supernovae can be separated using host brightness information and extendedness measures derived from the host's light profile. Next, we train a random forest model with data from **GHOST** to predict supernova class using exclusively host galaxy information and the radial offset of the supernova. We can distinguish SNe Ia and core collapse supernovae with $\sim 70\%$ accuracy without any photometric data from the event itself. Vera C. Rubin Observatory will usher in a new era of transient population studies, demanding improved photometric tools for rapid identification and classification of transient events. By identifying the host features with high discriminatory power, we will maintain SN sample purities and continue to identify scientifically relevant events as data volumes increase. The **GHOST** database and our corresponding software for associating transients with host galaxies are both publicly available.

Keywords: cosmology; observations; supernovae; machine learning; random forests

1. INTRODUCTION

In wide-fast-deep mode, Vera C. Rubin Observatory's (Vera Rubin Obs.; Ivezić et al. 2019) Legacy Survey for Space and Time (LSST) will image the entire Southern sky every ~ 4 nights. Much of this data will be rich in transient activity, with a predicted annual detection rate of 100,000 luminous supernovae. Type Ia supernovae (SNe Ia) will be especially valuable, as their standardizability make them ideal for measuring cosmological distances and tracing the expansion history of the Universe. Since their initial aid in the discovery of accelerated expansion (Riess et al. 1998; Perlmutter et al. 1999), SN Ia samples have placed strong constraints on both the dark energy equation of state (parameterized by w) and its potential evolution with redshift (Scolnic et al. 2018; Jones et al. 2018a).

LSST will discover supernovae photometrically, and retaining sample purities for photometrically classified SN Ia samples is an ever growing challenge. Contamination from Ib and Ic core collapse supernovae, whose light curves closely resemble those of SNe Ia, systematically biases derived estimates for w toward a time-evolving dark energy equation of state. A select few supernovae discovered by LSST will be prioritized for rapid follow-up on smaller telescopes, where high-cadence spectroscopy can aid in classification and progenitor studies, but we will first need accurate photometric classification to identify this scientifically valuable subset.

To address this issue, a concerted effort is now being directed toward the development of photometric classification software for supernovae and other transients. These classifiers primarily employ template fitting methods on real or simulated light curves (e.g. Poznanski et al. 2007; Karpenka et al. 2013), novel machine learning algorithms (Ishida & de Souza 2013;

Kimura et al. 2017; Muthukrishna et al. 2019; Möller & de Boissière 2020), or a combination of the two (Lochner et al. 2016). Community-wide challenges have also fostered development of photometric classifiers from outside the astronomical community, starting with the Supernova Photometric Classification Challenge (SNPhotCC; Kessler et al. 2010) in preparation for the Dark Energy Survey (DES) and the Photometric LSST Astronomical Time-Series Classification Challenge (PLAsTiCC; Kessler et al. 2019) in preparation for LSST. Many of these classifiers require the full phase coverage of photometric data for an event; during LSST operations, however, the sheer volume of alerts will require us to operate algorithms in real time on the alert stream itself. This has led to the creation of automated systems that rapidly ingest and process alerts from synoptic surveys, known as brokers. Examples of these brokers include ANTARES (Narayan et al. 2018) and LA-SAIR (Smith et al. 2019), and additional systems will be developed for early processing of massive data streams as new surveys come online.

Photometric classification at early times will be necessary not only for maintaining pure SN Ia samples, but also for studying the progenitor physics of rare events in detail (e.g. De et al. 2019; Hosseinzadeh et al. 2017; Jiang et al. 2017; Miller et al. 2020; among others). Several SNe Ia discovered at early times, including 2018oh (Dimitriadis et al. 2019; Shappee et al. 2019), have revealed flux excesses in the first few days after explosion, offering a unique probe into explosion shocks and potential interactions with non-degenerate companions. Fast-evolving luminous transients (FELTs) represent a novel class of events with light curve rise times as extreme as 2.2 days (for KSN2015K; Rest et al. 2018), and the number of fast transients discovered continues to be grow (Poznanski et al. 2010; Prentice et al. 2018; Tampo et al. 2020). Rubin will continue to push our explored parameter space to brighter cataclysmic events occurring across even shorter (< 1 day) timescales. Photometric classifiers that require the complete light curve of an event will be inadequate for understanding the progenitor physics of events within this parameter space; accurate real-time classification will be crucial. In an effort to bridge this gap, Muthukrishna et al. (2019) implemented a deep recurrent neural network for event classification, achieving a mean accuracy of 95% at early epochs in discriminating 12 transient classes before maximum. Despite early successes, the current generation of real-time classifiers trained on simulated data will be sensitive to shot noise in photometric measurements at early times. Further, despite the baseline cadence of LSST, revisits *using the same passband* are spaced be-

tween 10–20 nights in *grizy*, with even larger gaps in *u*. This presents a challenge for constraining the shape and color evolution of light curves of individual events, information upon which most classifiers depend. Prior information would decrease the dependence on these early and sparse observations and increase the robustness of these supernova classifiers.

Supernova classes have been known to trace galactic populations along the Hubble tuning fork in different proportions for decades (e.g. Oemler & Tinsley 1979). Type Ia supernovae occur more frequently in early-type, red galaxies with low star formation rates than in late-type, blue galaxies with high star formation rates (Foley & Mandel 2013; Hakobyan et al. 2014). In addition, Kelly & Kirshner (2012) suggest that SNe Ib/Ic are found mainly in metal-poor galaxies, and early-type galaxies hosting SNe II/Ib are on average bluer than early-type galaxies hosting SNe Ia (Suh et al. 2011). Correlations have also been identified between supernova type and both host galaxy morphology (Foley & Mandel 2013) and star formation rate (Kelly et al. 2014; Zhou et al. 2019).

Classification efforts can directly benefit from these host galaxy correlations. Foley & Mandel (2013) found that a Naïve Bayes classifier using *only* host galaxy morphology, absolute magnitude, color, galactic offset and pixel rank could classify supernovae as accurately as the best light curve methods of that time. Recently, Baldeschi et al. (2020) showed that photometric estimates of global star formation rate can be used to increase the purity of SN Ia and core collapse supernova samples by 10% and 20% from random, respectively. Our classifier achieves higher accuracy than these previous methods while exploring a complete parameter space of host features. The single-visit depth of LSST ($r \sim 24.5$ mag) will allow us to identify transient host galaxies within redshift ~ 1 , and we can use the complex host galaxy information collected by the survey as *a priori* data to better inform our classification efforts.

A thorough understanding of the dominant correlations between transient and host galaxy will also allow us to better correct for systematic effects within SN Ia data. SN Ia explosions are known to be influenced by their host environments, and metallicity (Höflich et al. 2010) and extinction from dust (Mandel et al. 2017) can change the shape and peak magnitude of the resultant light curve, respectively. Moreover, many groups have identified correlations between SN Ia Hubble Residuals and global properties of the host galaxy, including morphology, metallicity, and star formation rate derived from ground-based SDSS and Gemini observations (e.g. Hamuy et al. 1996; D’Andrea et al. 2011; Henne et al.

2017; among others). The global correlations identified to date are weak, and a more comprehensive approach would involve studying a wider range of host galaxy properties as well as correlations at the local scale; however, the paucity of higher resolution imaging has limited SN host galaxy studies at the pixel level and for a more exhaustive search of the feature space. The limitation of current host galaxy correlations in correcting for these Hubble residuals has resulted in an *ad hoc* piecewise “Hubble-mass-step” correction (Kelly et al. 2010; Sullivan et al. 2010; Lampeitl et al. 2010; Kim et al. 2014). With better constraints on SN Ia-host environment relations, physically motivated corrections could be incorporated into the SN Ia model to infer more accurate distances.

The SN Ia mass-luminosity correlation has persisted within growing sample sizes, and will remain even as other systematic effects are addressed by Rubin’s all-sky photometric calibration. It will soon become a dominant source of uncertainty (Scolnic et al. 2018). Characterizing these correlations now will be essential for placing tighter constraints on cosmological parameters in future surveys. With the ability to constrain and remove these systematic host environment correlations from the estimated fitting parameters of SN Ia light curves, we will strengthen our ability to probe dark energy and the expansion rate of the universe.

In this work, we explore the utility of host galaxy information in classifying supernovae. We extend the work done by Foley & Mandel (2013) by constructing a dataset of host-supernova pairs greater than an order of magnitude larger than the Lick Observatory Supernova Search (LOSS) sample they use; we also consider > 140 additional host galaxy features for classifying supernovae. In addition to our data products, we have developed a new method for supernova host galaxy identification in deep surveys using postage stamps of the field. This method achieves accuracies superior to the commonly used directional light radius method at low- z , and with greater completeness at high- z where little morphological information is available. This pipeline for host galaxy association will soon be integrated into the alert stream of the Young Supernova Experiment (YSE), which observes a total survey area of 1500 square degrees in two bands per epoch to discover and study supernovae before peak brightness (Jones et al. 2019; Jones et al. 2020).

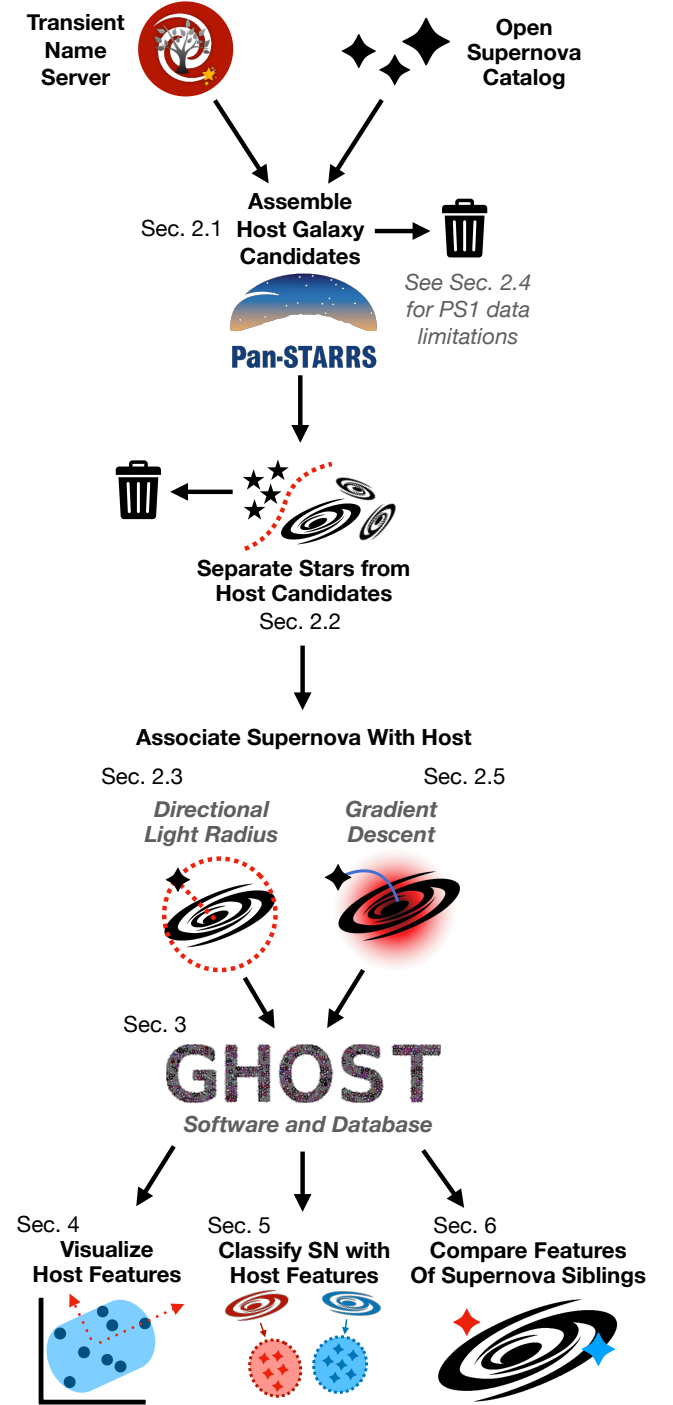


Figure 1. An outline of the analysis completed in this work, with corresponding sections labeled. The primary data sources for our supernova sample are given at the top of the flowchart, and major steps within our pipeline are indicated with text.

1.1. Structure of this Paper

We provide a schematic overview of this work in Figure 1. Our paper is laid out as follows: In §2, we describe our methodology for constructing and validating our database of supernovae and their host galaxies. In §3 we outline the data and software products that we have made public to accompany this work. These products can be used to query the released database and identify new supernova hosts. We compare PS1-derived brightness and morphology features of supernova hosts using Principal Component Analysis in §4. Next, we introduce our algorithm to classify supernovae from host galaxy information and present results in §5. Section §6 is devoted to the analysis of supernovae originating in the same host galaxy. We then compare the host galaxies of underrepresented supernova classes using t-Distributed Stochastic Neighbor Embedding (tSNE) in §7. We conclude by summarizing our results in §8 and discussing future directions for the research in §9.

2. HOST GALAXY IDENTIFICATION

To construct a dataset of supernova host galaxies, we must first assemble a dataset of previously discovered supernovae. We have downloaded all spectroscopically classified supernovae from the Transient Name Server (TNS; <https://wis-tns.weizmann.ac.il/>) and the Open Supernova Catalog (OSC; <https://sne.space/>). After removing duplicates identified by name and position, we are left with 20,736 events. We implement a series of quality cuts and a novel matching algorithm to identify the host galaxies of supernovae in our sample, and remove events without an associated host galaxy. Our final database contains 16,175 supernovae and their host galaxies, or just over 78% of all spectroscopically classified supernovae at the time of writing. We outline our methodology for matching supernovae with their host galaxies below.

2.1. PS1 Querying for Host Candidates

We use the first data release of Pan-STARRS (PS1; Chambers et al. 2016) to search for candidate host galaxies due to its survey depth ($5\sigma < 23.3$ in g -band) and extensive list of sources ($>3B$ unique objects). We have chosen Pan-STARRS data over SDSS for its superior sky coverage with comparable depth (SDSS has a median 5σ depth of 23.13 in g), and over alternative sky surveys for its resolution ($0.25''/\text{px}$, two orders of magnitude higher than the $21''/\text{px}$ resolution of the Transiting Exoplanet Survey Satellite). We opt for the first data release to take advantage of its *bestDetection* flag; these entries were corrupted in DR2.

To first order, a transient host galaxy can be identified by cross-matching the redshift of the event with the redshifts of nearby sources; however, the majority of supernova events reported to the Transient Name Server prior to 2010 do not report redshift information, and the NASA Extragalactic Database (NED¹) is only 75% complete for redshifts of galaxies at $z \leq 0.05$ and less complete for dimmer galaxies at higher redshifts (Kulkarni et al. 2018). For this reason, supernovae and their host galaxies cannot be associated by redshift alone. For each transient event, we construct a table of potential host galaxies using the following procedure:

1. Query Pan-STARRS for all catalogued objects within $30''$ of the supernova. If a host galaxy has been reported in TNS or OSC, we instead take its coordinates as the center of our cone search. The resultant table is likely to contain artifacts and other objects that are irrelevant to this analysis, such as HII regions.
2. Use the PS1 *primaryDetection* = 1 flag to remove duplicate detections of the same source, as is the case for fields containing a single large galaxy with a spatially resolved core or many associated HII regions. Several distant galaxies were identified without an associated primary detection, and so we caution that this step is likely to preferentially associate supernovae with nearby large galaxies.
3. Remove any object not detected in *gri*. We have found that the number of artifacts in our candidate host galaxy list increase dramatically without this cut, and we do not cut on z or y bands in order to retain high- z host galaxies in our sample.
4. Remove *bestDetection* = 0 sources if a source with *bestDetection* = 1 is present in the field. If there existed no best detection sources in the field, do not eliminate any potential host galaxies for that supernova. We had initially removed all sources with *bestDetection* = 0, but found that this removed a non-negligible fraction of plausible host galaxies.
5. Remove sources with *qualityFlag* = 128 (indicating a poor-quality stack object).

We list the fraction of supernovae removed at each of these steps in Table 2.5. After removing the majority of artifacts from our table, we eliminate the PS1 sources corresponding to stars.

¹ <https://ned.ipac.caltech.edu/>

2.2. Star/Galaxy Separation for Deep Surveys

Source brightness as measured in different apertures is a useful discriminator of point-like and extended sources (Slater et al. 2020). The total flux of unresolved sources is captured equally well by a point-spread function (PSF) model or by a more complicated aperture model such as Kron, which defines an aperture radius as $2.5 \times$ the first radial moment of a source (Magnier et al. 2016). For this reason, star-galaxy separation can be achieved to first order with a horizontal cut in $m_{\text{PSF}} - m_{\text{Kron}}$ space (See section 6.3 of Chambers et al. 2016), where stars will cluster along a $m_{\text{PSF}} - m_{\text{Kron}} = 0$ line. This cut introduces a bias against high-redshift galaxies that are nearly point-like, which are well-mixed with stars in this space faintward of $m_{\text{PSF}} \sim 21$. Further, stars brighter than $\sim m_{\text{PSF}} = 15$ will shift upwards of this line from saturation, and a horizontal cut will not remove these bright sources from our sample.

To more accurately remove stars from our list of potential host galaxies, we first search NED for every potential sources within our reduced list. Object classifications in the NED database are taken from their original literature sources, such as the Third Reference Catalog of Bright Galaxies (Corwin et al. 1994). Out of $>50,000$ unique sources, nearly 40,000 have classifications reported in NED. To classify the remaining 10,000 objects, we train a Support Vector Machine (SVM; Cortes & Vapnik 1995) to separate stars and galaxies using features of sources with NED associations. SVM is a supervised learning method that determines the separating hyperplane between model classes that maximizes the separation between similar values of distinct classes (the support vectors). Because NED labels are taken directly from literature, we can use them to construct an accurate training sample that incorporates domain-level expertise of each object. We implement our SVM model with the package `sklearn`, using a regularization parameter of 1 and a polynomial kernel of order 3.

We train our SVM model on the aperture magnitude (m_{Ap}) of our potential host galaxies in g , r , and i bands; $m_{\text{Ap}} - m_{\text{Kron}}$ magnitude in the same bands; and the 4-dimensional color distance in $g - r$, $r - i$, $i - z$, and $z - y$ from the PS1 stellar locus, the path traced by stars in color-color space. Because of its generality, the stellar locus is a valuable tool for photometric calibration of large surveys (High et al. 2009). We can also use it to aid in discriminating source types, since stars within our sample should closely follow this track whereas galaxies will not. Aperture magnitude for a source is determined by integrating over the analytic PSF aperture, then extrapolating the PSF model to estimate the flux not captured by the aperture. We have chosen this measurement in

place of m_{PSF} because we have found its values to have less dispersion (see Fig. 3), as it accounts for local variations in the PSF. We adopt a cubic spline with knots given by Tonry et al. (2012), with points in color-color space sampled with an $r - i$ bin width of 0.001, as our PS1 stellar locus. To calculate the 4-dimensional distance of each host galaxy from this locus, we use the equation (Covey et al. 2007):

$$4DCD = \min_k \sum_{i=0}^4 \frac{(C_i - t_{i,k})^2}{\sigma_i^2} \quad (1)$$

where C_i represents the source value of the i th color, $t_{i,k}$ represents each value along the stellar locus for that color, and σ_i represents the PS1 uncertainty in the color (added in quadrature from the uncertainties of the aperture magnitudes in the two bands). The $4DCD$ is found by the minimum value of this equation calculated for all k points along the stellar locus. This value approaches the orthogonal distance between a source and the stellar locus in 4D space as the number of discretized locus points approaches infinity.

We considered the use of Gaia DR2 parallaxes as an additional feature within our SVM, as it would allow us to distinguish between galactic stars and distant galaxies; however, the depth of the survey (with a limiting magnitude of $G = 21$) ensures that data is missing for a significant number of our sources. Further, the parallaxes that are reported in DR2 have significant uncertainties, so training our SVM to identify sources with large parallaxes as stars would remove a non-negligible fraction of galaxies from our sample as well.

Our SVM model allows us to recover realistic spreads for overlapping stars and galaxies in $m_{\text{Ap}} - m_{\text{Kron}}$ space, and retain potential high-redshift host galaxies in our sample. We show the distribution of stars and galaxies after this step, as well as their distribution along the PS1 stellar locus, in Figure 2.

We then remove the NED-identified stars and the SVM-predicted stars from our table of potential host galaxies. Of course, there are more objects than stars and galaxies in our list of PS1 sources. We have additionally removed objects identified as UV sources, HII regions, supernovae and supernova remnants (as are present in some postage stamps for more recent events), and white dwarfs. We do not remove infrared sources from our potential host galaxy list, as these could indicate host galaxies with strong infrared emission. Galaxies with the smallest separation from the stellar locus and the stars with the largest locus separation were inspected using PS1 postage stamps, but no manual re-association was done at this stage. The galaxies with smallest separation to the locus were nearly point

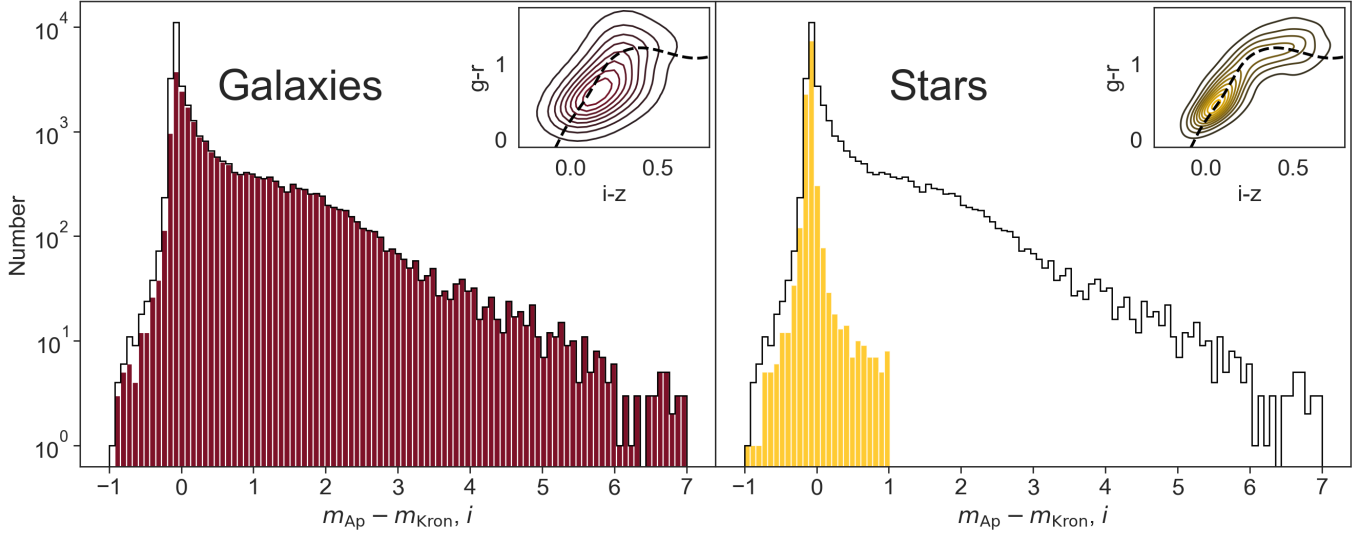


Figure 2. **Left.** A histogram in i -band $m_{\text{Ap}} - m_{\text{Kron},i}$ Magnitude space for the NED-identified and SVM-identified galaxies. The black outline represents the entire sample of stars and galaxies. We plot density contours for this galaxy data in color-color space top right, with a dashed line for the stellar locus from [Tonry et al. \(2012\)](#) (see §2.2). Galaxies within our sample do not closely trace the stellar locus, and sources closest to it (with low $4DCD$ values) were visually verified. **Right.** A histogram for the combined sample of NED and SVM-identified stars. Realistic tails for each distribution are recovered using our method, and objects within these tails were later manually verified with postage stamps from PS1. Truncating our sample near $m_{\text{Ap}} - m_{\text{Kron}} = 0$ would have removed a substantial fraction of potential high-redshift host galaxies from our sample. As before, we plot stellar density contours along with the PS1 stellar locus. These contours trace the stellar locus much more closely than our galactic sources, with a turnover near $i - z = 0.5$; no turnover is seen in the plot at left.

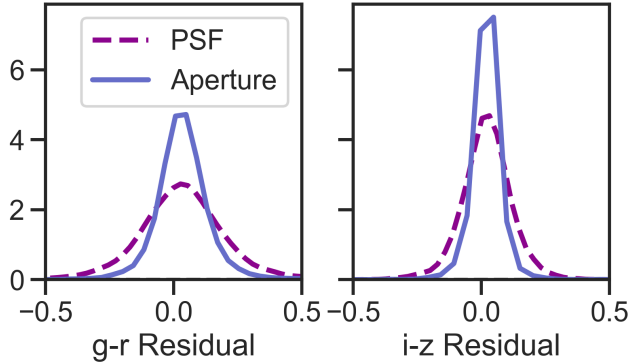


Figure 3. The residuals in $g - r$ and $i - z$ colors calculated between the PS1 stellar locus and identified stars within our candidate host galaxy table. Colors have been corrected for extinction using the reddening values and extinction coefficients from [Schlafly & Finkbeiner \(2011\)](#).

sources, but were kept in the dataset on the possibility that they were QSOs.

2.3. The Directional Light Radius for Host Galaxy Association

Supernovae are often associated with a host galaxy using the directional light radius (DLR) prescription outlined in [Gupta et al. \(2016\)](#), where the angular distance to each host θ is scaled by the radius of the host galaxy in the direction of the transient d_{DLR} . A supernova embed-

ded in a large galaxy is more likely to be found further from its host galaxy's nucleus than a small galaxy, and this normalized distance permits a direct comparison of supernova separations between host galaxies with vastly different scales. Normalized separation metrics have already been adopted by the Supernova Legacy Survey (SNLS; [Sullivan et al. 2006](#)) and the SDSS-II Supernova Survey (SDSS-SNS; [Sako et al. 2018](#)). As the rate of supernova detections continues to increase, the success of the DLR method at low- z and in crowded fields has made it the preferred method for automated host galaxy association (see [Gupta et al. 2016](#) for a detailed review).

The DLR method proceeds as follows. For a supernova located at coordinates $(x_{\text{SN}}, y_{\text{SN}})$ and a potential host galaxy located at coordinates $(x_{\text{Gal}}, y_{\text{Gal}})$, the Stokes parameters U and Q of the galaxy are given by its flux-weighted second order moments in PS1:

$$U = M_{XY}; \quad Q = M_{XX} - M_{YY} \quad (2)$$

The angular tilt of the galaxy relative to celestial north ϕ is then found with

$$\phi = \frac{1}{2} \tan^{-1}(U/Q) \quad (3)$$

Next, we calculate the aspect ratio of the host galaxy with

$$r_{a/b} = \frac{(1 + \kappa + 2\sqrt{\kappa})}{1 - \kappa} \quad (4)$$

where κ is derived from the two Stokes parameters:

$$\kappa = Q^2 + U^2 \quad (5)$$

The angle γ , describing the angle of the supernova position relative to the galactic center and celestial north, is then found with

$$\gamma = \tan^{-1} \frac{y_{SN} - y_{Gal}}{x_{SN} - x_{Gal}} \quad (6)$$

Finally, we arrive at the angle β subtended by the galactic semi-major axis and the vector connecting the supernova to the galactic center:

$$\beta = \phi - \gamma$$

The DLR is found with these parameters using the equation

$$d_{DLR} = \frac{r_a}{\sqrt{(r_{a/b} \sin \beta)^2 + (\cos \beta)^2}} \quad (7)$$

The scaled directional light radius is found by θ/d_{DLR} , where θ is the Great Circle distance of a supernova from the center of its host galaxy in arcseconds. An illustration of this method is given in Figure 4.

The DLR method uses second-order moments for estimating U and Q , which are model independent; however, an estimate of the host galaxy’s semi-major axis r_a must also be provided in Equation 7, and this may require us to adopt a light profile model for the galaxy. We have selected the Kron radius, defined as $2.5\times$ the first radial moment of a candidate host galaxy’s surface brightness profile, in the band which has the highest SNR, as our value for r_a to minimize this dependence. The mean r -band Kron radius for all potential host galaxies at this stage is $7.5''$.

Gupta (2013) estimates that 7% of matches in his sample generated using this method are erroneous, with an additional 3% of SNe left unassociated due to unreported second order moments. Using a naive DLR association, we find our fraction to be significantly higher due to the presence of additional non-galaxy sources in our database and multiple PS1 entries for a single source, which were only partially removed in previous steps. To mitigate this issue, we have implemented a modified DLR method. For each supernova in our sample, we implement the following steps:

1. Find the Kron radius of each potential host galaxy in the band with highest SNR. Then, calculate d_{DLR} . If either the Kron radius or the second-order moments are not provided, remove this source from the list of potential host galaxies. Repeat for all potential host galaxies.

2. Eliminate host galaxies with $\theta/d_{DLR} > 5$. If no host galaxies remain after this step, the supernova is reported to be hostless and added to the sample of hostless events.
3. Rank-order the host galaxies by ascending values of θ/d_{DLR} .
4. If the remaining list contains at least one NED-identified galaxy, select the galaxy with the lowest θ/d_{DLR} as host. If not, select the source with the lowest θ/d_{DLR} .

2.4. Limitations in the DLR Methodology Applied to PS1 Data

We have taken advantage of the depth of PS1 to construct a complete list of supernova host galaxies, but maintaining a catalogue as extensive as PS1 can also lead to several issues that we have encountered during this work. First, de-blending errors plague many of the low- z host galaxies in our sample. These objects are often described by several overlapping PS1 “sources”, and neither the *primaryDetection* nor the *bestDetection* flags were able to unambiguously identify the PS1 entry closest to the true SN host galaxy in all cases. Because of the de-blending errors associated with highly extended sources, we also find non-physical Kron radius measurements for the majority of these sources.

Second, deep PS1 imaging is able to resolve dimmer host galaxy features that would be missed in other surveys. This introduces additional “sources” to the list of candidate host galaxies for a supernova, further crowding low-redshift fields. We have often found a PS1 source at or near the true galactic center with a Kron radius (if one is reported in any band) that is uncharacteristically low for the galaxy, whereas sub-structures such as HII regions and bright stars may “adopt” the light profile of the entire galaxy and report uncharacteristically high Kron radius values. This issue biases the DLR algorithm *away* from large host galaxies where visual association would be trivial.

Third, high-redshift host galaxies can easily be mistaken for imaging artifacts, and are preferentially removed by the *bestDetection* flag. The Kron radius for these objects is often (understandably) not reported. This leads to an overabundance of unassociated supernovae in sparse fields.

We have attempted to develop a pipeline that is fault-tolerant to these limitations in PS1 data, but the success of the DLR method depends upon robust radius estimates for distinct sources in crowded fields. Gupta (2013) uses a cutoff value of $\theta/d_{DLR} = 4$ as a balance between sample purity and efficiency. We have extended

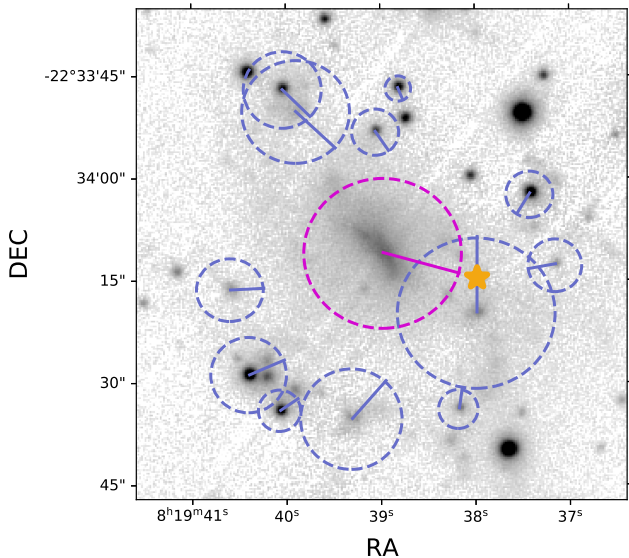


Figure 4. The PS1 postage stamp for SN 2014dp, with host galaxy candidates circled. We show the radius of each candidate in the direction of the transient, calculated using the Kron radius of the host galaxy and the DLR method in §2.3. Despite the center of the true host galaxy lying further from the transient event than other spurious candidates, the true host galaxy (magenta) is correctly identified using our modified DLR method. The match is verified using redshift information from NED.

this value to 5 to account for the low Kron radius estimates associated with low-redshift host galaxies; we note that a similar threshold is used for associating host galaxies in SNLS (Sullivan et al. 2006).

By visually inspecting a random subset of associated host galaxies, we predict our overall matching error rate with the full pipeline to be $\sim 5\%$; however, for low-redshift objects our error rate can in some cases be as high as 30% for the reasons given above. In the cases where DLR has failed, a supernova is often matched to an HII region or bright star. To maintain the accuracy of our associations for spatially extended sources, as well as for high- z host galaxies, we have developed a novel host galaxy association algorithm using the light profiles of sources nearest the supernova of interest. We provide a detailed description of this method below.

2.5. Host Galaxy Association using Background Image Gradients

While deep imaging of extended host galaxies in PS1 makes source de-blending challenging, it also makes visual association of SN host galaxies easier. We can rapidly identify a host galaxy by eye by first identifying whether the supernova is embedded within an ambient light profile brighter than the sky background and, if so,

by tracing this profile from the location of the supernova to the location of a nearby host.

We have automated this process with a gradient ascent method able to accurately locate the center of the host galaxy in which a cataclysmic event is embedded. We release this code with the rest of the GHOST software outlined above.

For each transient, we have downloaded an 800x800 pixel ($200'' \times 200''$) postage stamp of the field in *gri*. We have also downloaded the corresponding PS1 image stack masks and number counts. We use the stack masks to remove saturated pixels such as those corresponding to stars, and the counts mask to remove pixels created from fewer than two images in the stack. To remove stars that have not saturated the detector and any remaining starlight from those that have, we use the DAOSTarFinder routine within the *astropy* package *photutils* to identify sources matching a gaussian light profile with $\text{FWHM} \sim 3$ at a threshold of 20 standard deviations above the median pixel intensity. We have intentionally set our threshold high in order to prevent masking AGN at the centers of galaxies, as these provide meaningful gradient information. We then remove each identified star with a circular mask of radius 5 pixels.

Once we have identified and removed stars from the field, we use *Scipy* to construct a two-dimensional cubic spline interpolation on the pixels that were previously masked. We apply the zero-points to these *gri* images, average these three source-removed postage stamps in magnitude space, and convert back to flux to generate a PS1-averaged image *A*. Next, we use the *astropy* package *photutils* to estimate the background of image *A*. This tool is usually used to remove background gradients from a crowded field (such as those caused by massive galaxies) and study smaller sources in detail, but for this method we are interested in the background gradients themselves. By considering the background estimated by *photutils* and not subtracting it from the postage stamp, we are able to create an image dominated by the galaxy light profiles in *A* and containing minimal remaining effects from dust and HII regions. This resultant image, *B*, forms the basis for our gradient ascent method.

To estimate the sky background in a field, we divide a pointing into identical smaller regions, apply a median filter across each smaller region, then interpolate the resulting pixels back to the resolution of the original postage stamp. This smoothing requires a careful selection of both the size of each sub-region, or box, and the size of the median filter applied within each sub-region. Ideally, the size of each box should be larger than the HII regions and other galactic structure mak-

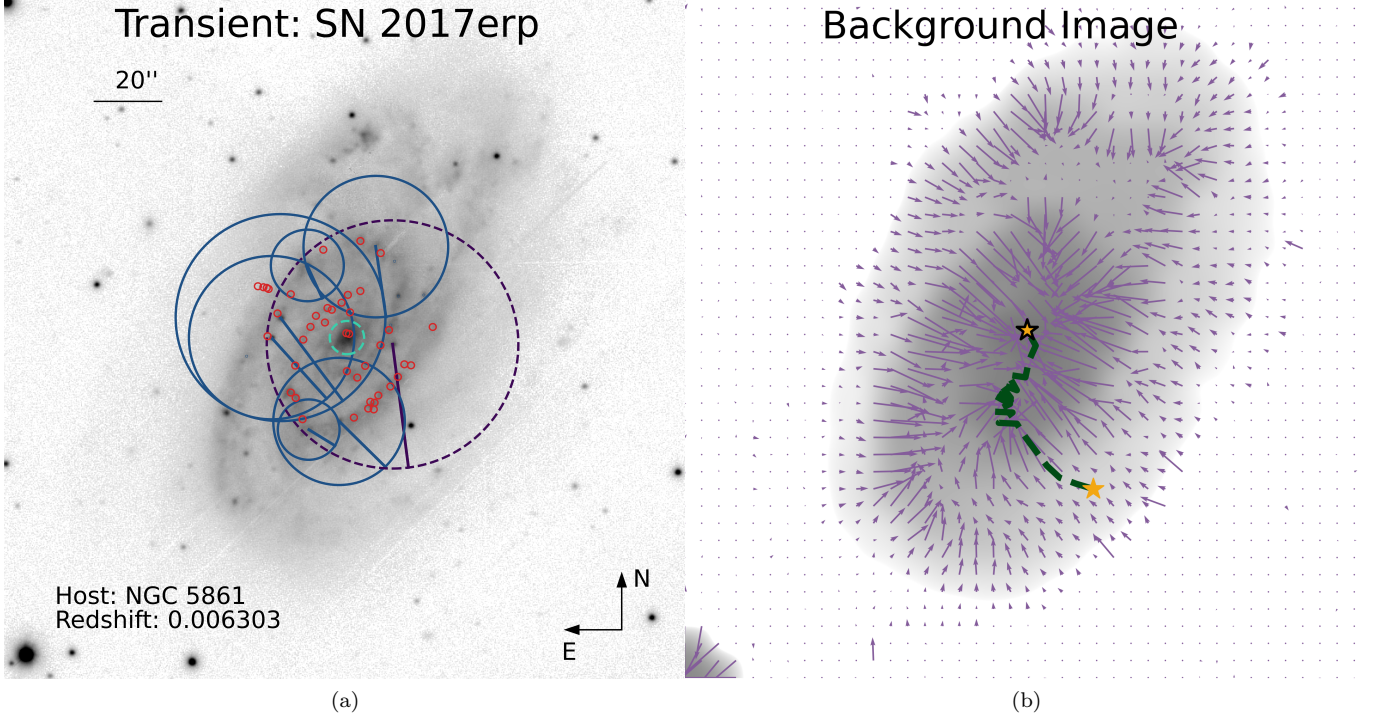


Figure 5. **a.** The gradient ascent algorithm applied to SN2017erp. The red circles correspond to the positions of PS1 sources eliminated before the DLR calculation, while the blue circles (scaled by d_{DLR}) denote potential host galaxies at the DLR stage. The dashed purple circle denotes the DLR-selected host galaxy, while the smaller dashed green circle at center denotes the PS1 source selected by gradient ascent. Despite numerous spurious detections in the field, the gradient ascent algorithm is able to rapidly identify the true host galaxy, which was later verified by redshift. **b.** The estimated background light profile of the central host galaxy, found by dividing the postage stamp into squares and applying a median filter to each of these sub-regions. We give the background pixel gradients, in purple, at every 20th pixel for clarity. The position of the supernova is given by the yellow star, and the star outlined in black marks the final location reached by the gradient ascent method. By masking saturated pixels and point-sources, we recover the light profile from the true host galaxy.

ing up the host galaxy of interest, and small enough to capture its radial light profile. A large sub-region and median filter will smooth local brightness variations; a small sub-region and median filter will preserve them. As a result, the size of the sub-region needed to resolve a host galaxy’s light profile will change drastically from field to field. We have empirically determined a set of criteria for predicting whether the true host galaxy will fall into three size categories - “small”, “medium”, or “large” - and these criteria determine the sizes of the image sub-regions and the median filter. A sub-region of 75x75 pixels is used for large host galaxies, while sub-regions of 40x40 and 15x15 px are used for medium and small host galaxies, respectively. The median filter used for large and medium host galaxies is 3x3 pixels; for small host galaxies, no filter is applied to the data.

The criteria for estimating the size of the true host galaxy are based upon four measurements:

1. \tilde{I} : The sigma-clipped median count of the image, which characterizes the flux of non-stellar light across the full postage stamp. A high value of

\tilde{I} suggests a large host galaxy in the field, but can also be biased by starlight.

2. f_{IM} : The fraction of pixels in the image with a photon count of at least unity. This metric provides additional evidence for a single extended source dominating the field, and is less biased by stellar saturation.
3. f_{SN} : The fraction of pixels within a 200x200 pixel box centered on the supernova with a photon count of at least unity. This provides strong evidence for the spatial extent of the true host galaxy. If both f_{SN} and f_{IM} are near unity, a host galaxy is deemed large; if f_{SN} is large but f_{IM} is small, a medium host galaxy is assumed.
4. I_{SN} : The image count at the location of the supernova. If this value is above a certain threshold, the host galaxy is deemed “small”. This may appear counterintuitive, but this designation suggests that the supernova occurred near its host galaxy center. In this case, it is important that

we use a small filter to preserve the location of the host galaxy center, regardless of the true host galaxy size.

We have found that a large filter can shift the location of a host galaxy center due to a combination of AGN masking and edge effects. To recover the local peak, we normalize and combine images A and B into a weighted average (image C) with weights determined by the magnitude of I_{SN} and the number of masked pixels in image A . Image B is given the dominant weighting in the resulting image unless I_{SN} is above a threshold, for the same reason described above. If more than 15% of the image has been masked, the cubic interpolation of the image becomes unreliable and artificial photon counts from interpolated masked stars contaminate A . In this case, the reference image A is given a weight of 0.

Once we have an estimated background image corresponding to our field, we estimate the two-dimensional gradient at each pixel using the `numpy` package, with second-order central differencing at the interior points and first-order differencing at the boundaries of each postage stamp. We begin at the location of our supernova $(x_i, y_i) = (x_{SN}, y_{SN})$ in pixel coordinates and update the position according to the image gradient $\nabla C(x_i, y_i)$, using a forward Euler updating scheme:

$$(x_{i+1}, y_{i+1}) = (x_i, y_i) + h \nabla C(x_i, y_i) \quad (8)$$

Here h represents a chosen step size. After completing a step, we convert our updated position coordinates to integer values and continue. The algorithm iterates until the calculated position has reached the edge of the postage stamp or for 1000 steps, whichever comes sooner. If the algorithm reaches a position with a gradient smaller than a pixel separation, it is perturbed one pixel in a random direction away from its current position. This feature, combined with the large number of total iterations, prevents the algorithm from getting trapped in a local maximum of the light profile. After the algorithm terminates, a PS1 cone search is done within $5''$ of the terminated position (or $20''$ if the host galaxy is assumed to be large). We eliminate sources from this list with only one detection across all bands, and then select the source closest to the terminated position that is not listed as a star in NED. By tracing the local gradient in the postage stamp, the algorithm “crawls” to local areas of increased brightness. For spatially extended sources, the gradients will cause the step to terminate at or near the center of the supernova’s host galaxy. We illustrate this algorithm in Figures 5a and 5b.

For this algorithm to be successful, we must place careful consideration into the selection of a physically relevant step size h . This must be large enough to “overlook” remaining deviations from a smooth light profile; while small enough to prevent overshooting the true center of a host galaxy. For each supernova, we calculate h as the product of the mean Kron radius for all remaining potential host galaxies in the field, and a scale factor based on the estimated size of the true host galaxy. This scale factor corrects for the tendency of PS1 Kron radius values to underestimate the true spatial extent of the host galaxy, described in greater detail in 2.4; if h is set to the mean Kron radius, the algorithm terminates before the galactic center is reached for the majority of fields.

We have run this algorithm on supernovae for which no host galaxy was found using DLR, as well as the supernovae for which at least one candidate host galaxy had incomplete morphological information. There are 2,137 supernovae matching the first criterion, and 3,129 matching the second. We find by visual inspection that the gradient ascent method achieves a 12% misassociation rate for the incomplete morphology sample, compared to 16% for the DLR method; and a $\sim 3\%$ misassociation rate for the no host galaxy sample, which generally consists of less crowded fields. More importantly, our method is able to recover 800 host galaxies from the hostless sample, nearly half of the supernovae removed by the DLR method and roughly 4% of all spectroscopic supernovae. We have included these matches in our final database.

We have found our gradient ascent method to reliably recover more transient host galaxies at low-redshift where a large galaxy dominates the field, and at high-redshift with sparse fields. When the host galaxy is large and the field is crowded, the large filter used for this method can blend multiple galaxies and shift the peak of the true host galaxy’s light profile. This causes the algorithm to terminate at an artificial maximum in the image, and can lead to incorrect associations.

After incorporating host galaxies matched with the gradient ascent method, we manually re-associate an additional 425 supernovae ($\sim 2.6\%$ of our table) by eye that were mismatched in our sample, and another 69 low- z supernovae (0.4% of our table) that were dropped at different stages in our association pipeline. We also identify misassociations by plotting the redshift of each supernova as a function of its angular separation θ from its host galaxy. Several of our associations have $\theta > 15''$ and $z > 0.1$, corresponding to a physical separation of > 30 kpc. Although supernovae have been discovered as far as 80 kpc from their host center owing to tidal

Pipeline Step	Fraction Removed	Total Fraction
PS1 30'' cone search for nearby host galaxies	7.3%	92.7%
Removal of sources not detected in <i>gri</i>	3.2%	89.5%
Removal of sources with <code>qualityFlag = 128, primaryDetection = 0, bestDetection = 0</code>	<0.1%	89.5%
Star, galaxy separation with SVM	3.6%	85.9%
Directional light radius host galaxy association	10.3%	75.6%
Gradient ascent host galaxy association	-3.9%	79.5%
Redshift mismatch	1.9%	77.6%
Manual reassociation	-0.4%	78.0%

Table 1. The fraction of total spectroscopically classified supernovae dropped from our table at each stage of our association pipeline. We also list the total SN fraction remaining in the database after each step.

interactions with other galaxies (Ferretti et al. 2017), events at this separation are likely to be uncommon (see Figure 2 of Galbany et al. 2012). To confirm this sample as misassociated, we identify the systems for which the redshift of the supernova differs from that of the host galaxy by greater than 50% of the supernova’s redshift. We plot this sample in Figure 6a. These ~ 300 events occur predominantly at $z > 0.1$ and comprise the majority of our high- z matches with large separation. We have removed these events from our database. As a result, we estimate the final misassociation rate of our database to be $< 3\%$, lower than the original association error rate provided by Gupta et al. (2016). We report the fraction of total supernovae dropped from our sample after each stage of the pipeline in Table 2.5.

Our final database contains identified host galaxies for 78% of all spectroscopically classified supernovae, higher than the completeness of SN candidate associations reported by Gupta (2013) (73%, or 15,826/21,787 candidates) and spanning a significantly wider range in redshifts. We are able to associate the majority of spectroscopic supernovae within $z < 0.62$, whereas the furthest supernova candidate in Gupta (2013) was at $z = 0.46$. Of our unassociated sample, 33.2% were located at declinations below -30° , where a host galaxy search was excluded because no PanSTARRS 3PI survey images would be available. Excluding these events from our total sample brings the fraction of associated supernovae to 84%. The redshifts of supernovae in the remaining unassociated sample are significantly higher than the redshifts of supernovae in the associated sample, as is shown in Fig. 6b; it is likely that even PS1 depths are insufficient to resolve these host galaxies.

We have identified 43 supernova pairs in our final table as duplicates with the same redshift, similar discovery dates (within 100 days of each other), and with coordinates matched to within 1 arcsec of each other, and removed them. Two supernovae were matched to within 1 arcsec but have discovery dates greater than one year

apart. This pair of events is SN007ie, a type Ia supernova discovered on May 9th, 2007 at an RA, Dec (J2000) of 334.4029, 0.6133; and PS1-11aqj, a type II supernova discovered on February 9th, 2011 at an RA and Dec of 334.4028, 0.6134.

3. DATA AND SOFTWARE PRODUCTS

3.1. The GHOST Database²

We have released our full database of 16,175 spectroscopically classified supernovae, as well as the derived properties of their identified host galaxies from PS1, as the Galaxies HOsting Supernova Transients (GHOST) database. The full table can be downloaded as a CSV, and the host galaxy data for OSC supernovae have been added to the JSON data files and re-released for convenience. We have also included photometric estimations of 1,436 host masses (Foundation, Foley et al. 2018; PS1COSMO, Scolnic et al. 2018, Jones et al. 2018a), Hubble residuals of 124 SNe Ia from Kaepora (Siebert et al. 2019), postage stamps of each host galaxy, host galaxy and transient spectra, and transient light curves where available. Supernova spectra have been scraped from TNS and host galaxy spectra are taken from the Sloan Digital Sky Survey (SDSS; York et al. 2000) and NED. In addition to the data, we have developed software for rapid querying of the catalogue and association of new host galaxies. We describe the functionality of the code in the following sections.

3.2. Analysis Tools for the GHOST Database

We have developed and released a Python package to accompany GHOST for analyzing the data products. It can be found at the repository for this work. The software also contains the full analysis pipeline used in this work for associating host galaxies with the modified DLR and the gradient ascent methods. The package contains several main functions or parsing the database.

² <https://github.com/alexandergagliano/GHOST>

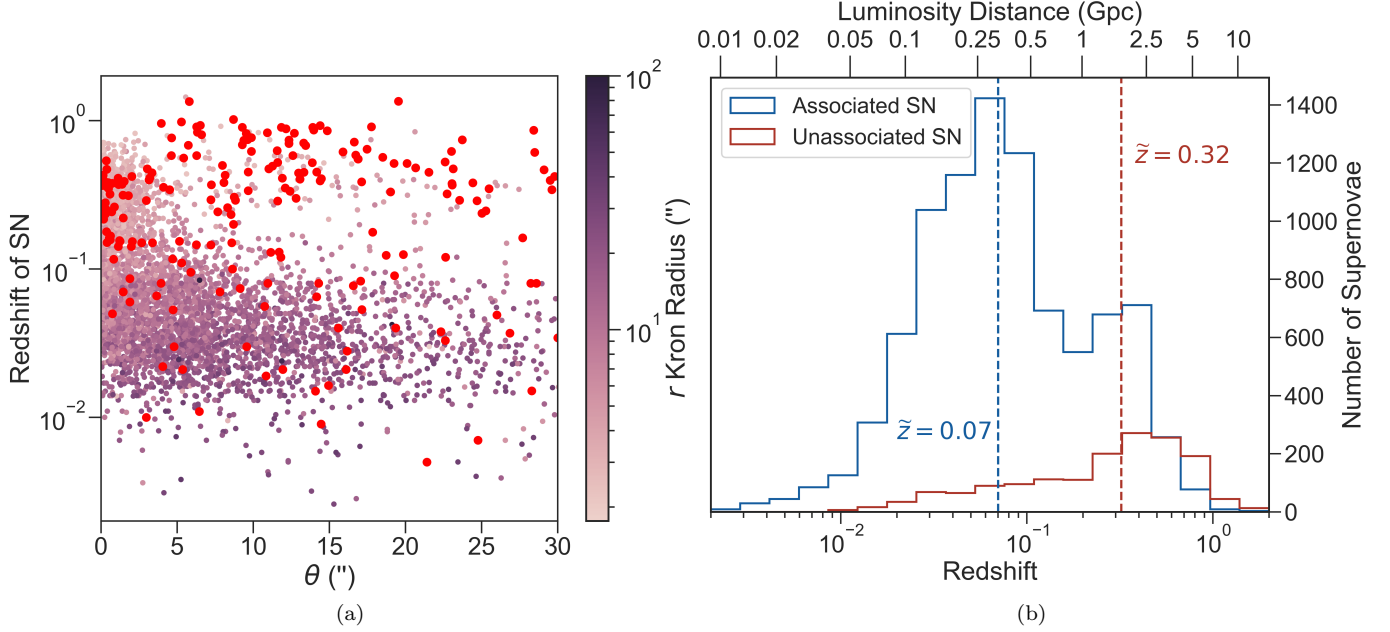


Figure 6. **a.** The redshifts of spectroscopic supernovae in our sample as a function of angular separation θ from their host galaxy, colored by the host galaxy's Kron radius in r . We find a θ distribution roughly matching that given in Galbany et al. (2012) but with multiple high- z host galaxies with $\theta > 15''$. In most of these high- z cases, the host galaxy's Kron radius is too small to reasonably explain this wide separation. By flagging the systems where the host galaxy's redshift differs by more than 50% of the supernova's redshift, this high- z sample is identified to be predominantly missassociated systems. **b.** The distribution of spectroscopic redshifts for supernovae with associated host galaxies in GHOST and those without identified host galaxies. The median of each distribution is shown. Assuming a standard cosmology ($H_0=67.8$, $\Omega_0 = 0.3$) and a flat Universe, the supernovae in our sample lie at a median luminosity distance of ≈ 318 Mpc, while the unassociated sample lies at a median luminosity distance of ≈ 1.7 Gpc. We are able to associate the majority of supernovae at each redshift bin before the bin centered at $z = 0.62$; the supernova sample analyzed in Gupta (2013) spanned the range $0.01 \leq z \leq 0.46$.

We provide the names and a basic description of these functions below:

- **getHostFromTransientCoords:** Inputs the location of the transient as an `astropy SkyCoord` object, and returns the host galaxy associated with that transient (if it exists in the database).
- **getHostFromTransientName:** Inputs the TNS name of a transient, and returns the associated host galaxy.
- **getHostStatsFromTransientCoords:** Inputs the location of the transient as an `astropy SkyCoord` object, and returns basic statistics about a host galaxy (including other associated transients in the database).
- **getHostStatsFromTransientName:** Inputs the TNS name of a transient, and returns basic statistics about a host galaxy.
- **getTransientStatsFromHostName:** Generates basic statistics for a transient (or a series of tran-

sients) based on the NED-reported name of its host galaxy.

- **getTransientStatsFromHostCoords:** Generates basic statistics for a transient, based on host galaxy location as a `astropy SkyCoord` object.
- **getHostImage:** Inputs a transient TNS name and returns a postage stamp of the most likely host galaxy in one of the PS1 bands - g, r, i, z, y - as a fits file, and plots the image in gri as a color image.
- **getTransientSpectra:** Plots the spectrum of the transient from TNS, if it is available.
- **getHostSpectra:** Plots the spectrum of the host galaxy from SDSS or NED.
- **coneSearchPairs:** Completes a cone search for all transient-host pairs whose transient location falls within a certain radius, returned as a pandas dataframe. Useful for identifying supernovae associated with the same system where the NED

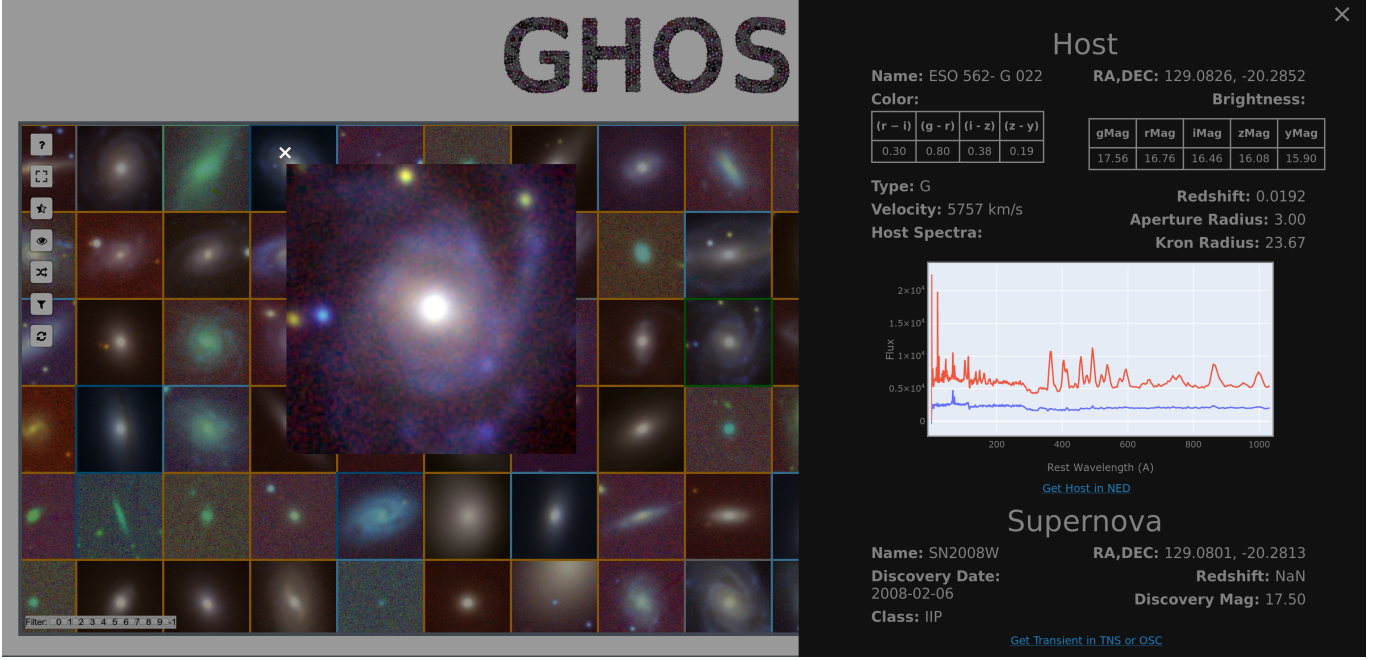


Figure 7. A screenshot of the **GHOS** Viewer, which consolidates 16,175 host galaxy postage stamps and basic information about the supernovae they host into a streamlined GUI. A pop-up sidebar provides spectra for both supernova and host galaxy, if they are available. Light curve data from the Open Supernova Catalog is also presented. By viewing many identified host galaxies simultaneously, incorrect associations can be rapidly identified and population statistics can be studied in greater detail.

name in the database is that of an HII region or star within the galaxy.

- **fullData:** Returns the full **GHOS** database.

Sample code outlining the usage of each of these functions, as well as the functions for associating new transients, is provided at the link above.

3.3. The *GHOS* Viewer³

We have also created a website for simultaneously viewing all host postage stamps in our database, which is hosted at the National Center for Supercomputing Applications (NCSA). Postage stamps are dynamically scaled in real time so that the user may rapidly view many host galaxies or individual systems of interest. Host galaxy images are color-coded by the class of the supernova matched to them. After selecting a postage stamp, a basic summary of both the supernova and its host galaxy are provided in a sidebar. Users may interactively search the **GHOS** database to find a specific supernova by its name, spectral class, or by the name of its host galaxy. Interactive plots showing the spectra of both host galaxy and supernova are also presented if available, and this data can be downloaded as a csv

table. Both **GHOS** and its associated viewer will be updated periodically as new supernovae are reported.

4. DIMENSIONALITY REDUCTION

Our final dataset contains 317 features of 16,175 PS1 sources, along with 7 features of their associated supernovae. Greater than half of these features characterize the PS1 detection of the source, including the pixel coordinates of the source in each filter, the number of source detections, and the detection ID in each band. Nevertheless, the number of remaining host galaxy features prohibits a brute-force search for supernova correlations. Further, galaxy features are well-known to be highly correlated with each other, leading to empirical relationships such as the color-magnitude relation (Bell et al. 2004) and the Fundamental Plane for ellipticals (Dressler et al. 1987). These properties can each reveal similar information about a galaxy’s position along an evolutionary track; consequently, these features may not each provide unique information about the class of a supernova.

To test this hypothesis, we construct a correlation matrix, given in Figure 8, for the galaxy features in **GHOS**. We use Spearman’s rank correlation over the Pearson correlation because the latter characterizes only linear relationships between features, whereas the former quantifies the ability of a relationship to be described by any monotonic function. For features repeated in

³ GHOS.ncsa.illinois.edu

each band, we have only shown those features in *g*. We find that over half of our galactic features in a single band are $> 80\%$ correlated, and the same features across multiple bands are even more strongly correlated. The strong correlations between magnitude, flux, and radial moments of sources in our host galaxy sample appear as blocks within the full correlation matrix. These blocks form a regular grid across our matrix due to the strong correlations between brightness features in each band. Aperture radius is not strongly correlated with our other photometric features, and therefore appears as a gap in the correlation blocks.

4.1. Identifying Dominant Host Galaxy Features with Principal Component Analysis

To reduce our list of host galaxy parameters without reducing their predictive power, we undertake a principal component analysis (PCA) of our galaxy data. In PCA, a dataset is transformed to a set of orthogonal components with the first principal component containing the most uncorrelated variance in the data. A dataset composed of features that are highly correlated with each other will be well explained by a single principal component, which is a linear combination of the original correlated features.

We begin by re-scaling our host galaxy features to each have a mean of 0 and a variance of 1. Each of these features is continuous instead of categorical, rendering one-hot encoding unnecessary. Re-scaling is necessary to directly compare features whose values may differ in both magnitude and range; if a single feature contains a wide range of values, the first calculated principal component will capture most of the variance in this feature alone and not across all features. Next, we transform our GHOST database to its first two principal components using the `sklearn` package in Python. We find that these principal components capture over half of the variation in our PS1 galaxy data (54%), confirming the degeneracy in individual features shown in Fig. 8.

A benefit of dimensionality reduction methods is the ability to visually inspect classes of objects as a function of many features. We present a biplot of our principal component model in Figure 9, along with the distributions of SN Ia, SN Ib/c, and SLSN host galaxies in this reduced space. Because the principal component axes are constructed from linear combinations of the galaxy features, we can represent the initial galaxy features from our data as vectors in this reduced space. The loading of each vector, defined as its length projected onto each PCA axis, describes the weight given to that feature in determining a principal component. Highly linearly correlated features are given similar weights along

the two axes, and we can see a clustering of magnitude features, flux features, and morphological features forming the dominant contributions to this PCA space. The first principal component, which explains 44.5% of the variation in host galaxy information, is determined nearly equally by the Kron radius of the source in each band, and its PSF, Kron, and Aperture magnitudes. The second principal component, which explains 10.4% of the variation, is determined mainly by the PSF Flux, *momentRH* (the square root of the first radial moment) and *ExtNSigma* in each band (a PS1 derived feature extremely similar to our $m_{\text{Ap}} - m_{\text{Kron}}$ mag, *ExtNSigma* is defined as the difference between PSF and Kron magnitude of a source subtracted by the stellar median value and divided by the error combined in quadrature; see [Magnier et al. 2016](#) for more information). The characteristics of SN Ia host galaxies are widely distributed in this space, with two distinct peaks at separate locations along both principal components. The host galaxies of SN Ib/c show significantly smaller variance, although with a significantly smaller sample size (591 SNe Ib/c vs. 6,279 SNe Ia) this lack of variation may be unphysical. These three classes are also centered at different locations in PC space, which can be used as a diagnostic tool for initial discrimination of supernova types without any information from the explosion itself.

The multimodal distribution of SN Ia host galaxies in this PCA space suggests multiple distinct populations, particularly given the large sample size of this class. In addition, the strong overlap of SN Ia host galaxies with both SN Ib/c and SLSN host galaxies suggests that SNe Ia may arise in host galaxies photometrically similar to galaxies that host either SNe Ib/c or SLSNe. By embedding characteristic postage stamps at each peak in Fig. 9, we can see that one SN Ia mode aligns with bright spiral galaxies (which are similar to SN Ib/c hosts), whereas the other aligns with faint, featureless hosts (which are similar to SLSN hosts). The bimodality of SN Ia host galaxies also presents a challenge for classification, with SN Ia galaxies at the left peak likely to be misclassified as hosting a SLSN and SN Ia galaxies at the right peak likely to be misclassified as hosting a SN Ib/c. Despite this overlap, the separation along the first principal component suggests that type information is revealed by host galaxy information alone.

By projecting our host galaxy features into a reduced space, we can also visually identify outliers within the GHOST sample. Fig. 9 reveals a sub-sample of SLSN outliers that are well-separated from the rest of the distribution in PCA space. This population is comprised of four supernovae in our dataset. Two of these are SN2213-1745 and SN2016aps, events whose

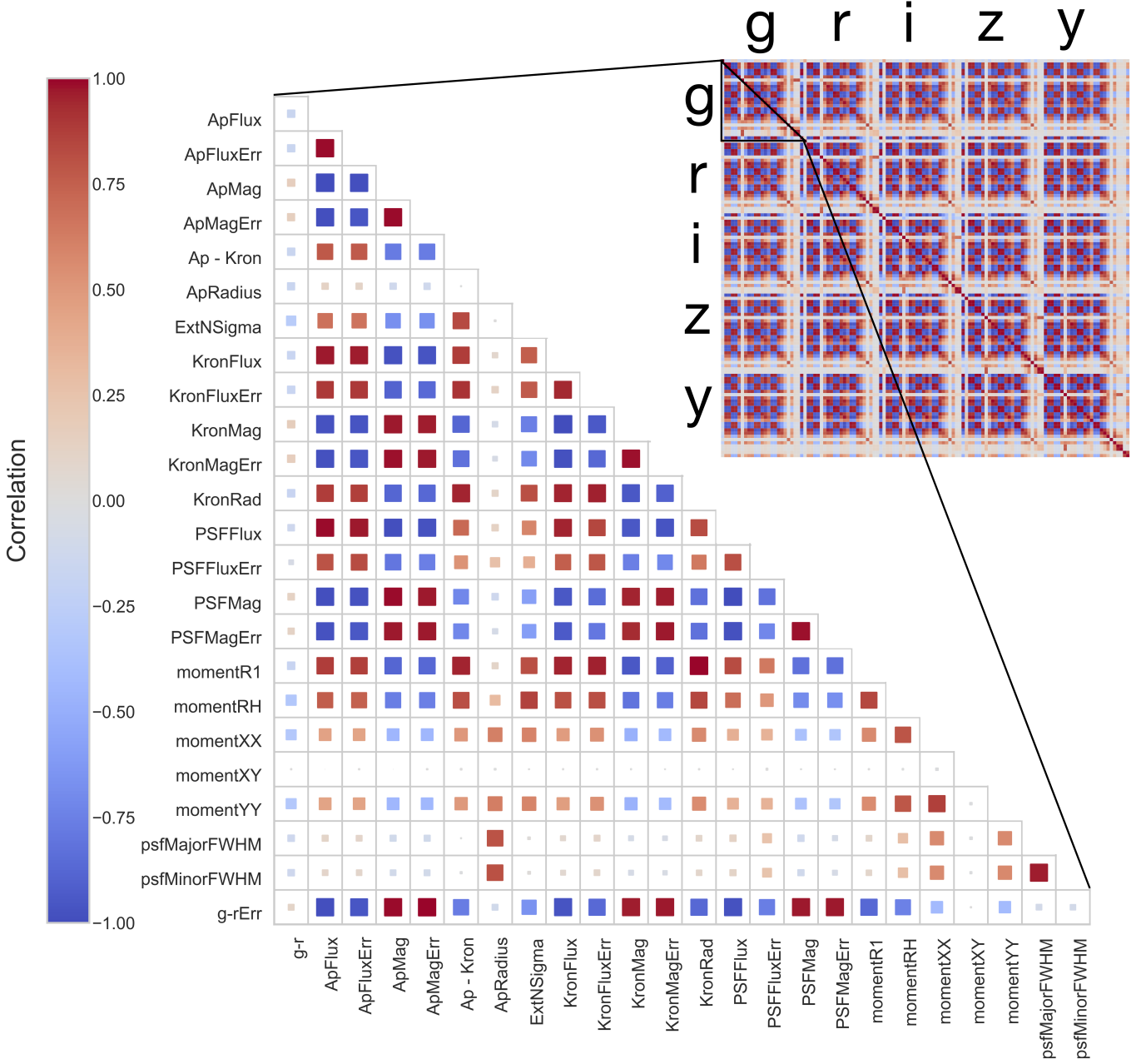


Figure 8. The Spearman rank correlation between PS1 features in a single band (g), with blue corresponding to negatively correlated features and red corresponding to positively correlated features. Over half of the features used in our random forest are strongly correlated with each other, particularly the magnitude of the host galaxy as measured in different apertures and its first and second order radial moments; strong correlations can also be seen in the same features across multiple bands (inset at right), leading to the block structure of the matrix. Because this matrix describes both linear and non-linear correlations, it is able to capture the relationship between flux and magnitude measured in different apertures.

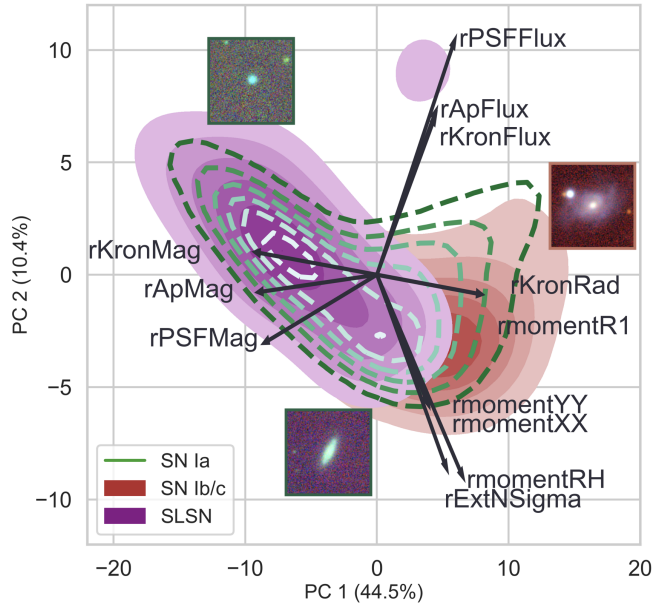


Figure 9. The distribution of host galaxy parameters for three supernova classes in our data, SN Ia, SN Ib/c, and SLSN, transformed into our reduced principal component space. For clarity, we plot in black only the feature vectors in r with highest loading along the two principal component axes. SN Ib/c and SLSN distributions are centered at different positions along the first principal component, suggesting associations with host galaxies with different size and brightness properties. The distribution of SN Ia host galaxies is bimodal, suggesting multiple host galaxy populations. Postage stamps for host galaxies associated with each peak of the SN Ia distribution are inset, as is the host galaxy located at the peak of the SN Ib/c distribution at right.

hyper-energetic explosions make them strong candidates for pair-instability or pulsational pair-instability supernovae (Cooke et al. 2012; Nicholl et al. 2020). SN2016aps is the brightest supernova ever discovered, with peak absolute magnitude of -22.35 ± 0.09 in i . Another supernova in this sample is SN2017gci, which was listed in the original AT report as a candidate cataclysmic variable; and LSQ14fxj, which has been alternatively classified as a SLSN, SN Ic, and an unusually bright Ia by different groups. From the feature loadings in Fig. 9, it is possible that some of these events correspond to the faintest SLSN host galaxies in our sample; indeed, SN2017gci was initially listed as hostless, and the estimated redshift of SN2213-1745 is $z = 2.0458 \pm 0.0005$ (Cooke et al. 2012), making it the most distant SN in our sample. The fact that these rare supernovae are also associated with outliers in our host galaxy sample suggests a strong correlation with their host galaxy, and studying these host galaxies in more detail will likely shed light on these enigmatic events.

Because significantly more information from our full table is captured by the first PCA component, we can better visualize the variance between classes by projecting it along only this axis. A ridgeplot is shown in Fig. 10 for our full data (without re-balancing classes), which plots Gaussian kernel density estimates (KDE) of each class. Because sample size varies dramatically among the classes plotted, the spread in each may not be representative of the true underlying population for each class; however, the relative positions of the medians of each distribution are illustrative.

Broadly categorizing this principal component as “size and brightness” and the second principal component as “light profile” in alignment with the loadings from Figure 9, we see systematic differences between multiple classes. The distributions of host galaxy parameters for type II, Ib/c, and IIB supernovae peak at nearly the same location and feature a heavy rightward skew, a strong indication that these supernovae are found in host galaxies with similar light profiles and Kron radii. These distributions appear distinct from that of SLSN host galaxies (comprised of an equal number of SLSNe-I and SLSNe-II, with a strong leftward skew; and that of Ia supernovae, without a strong skew in either direction. By visually inspecting a subset of the postage stamps corresponding to these populations, we find our SN Ib/c and SN II samples to consist mainly of large spirals, whereas our SLSNe are hosted in smaller galaxies with a range of different morphologies. Visual inspection of our SN Ia host galaxy sample did not reveal any consistent trends with respect to size or morphology, potentially explaining the wide spread of the SN Ia KDE. This suggests that the horizontal axis in Figure 10 corresponds roughly to brighter, larger galaxies toward the right and smaller, fainter galaxies toward the left. These results are in agreement with previous findings that SLSNe-I are found almost exclusively in low-mass dwarf galaxies with low star formation rates (Perley et al. 2016; Leloudas et al. 2015; Lunnan et al. 2015; Angus et al. 2016), whereas core collapse supernovae occur predominantly in late-type galaxies with high star formation rates (Cappellaro et al. 1999; Hamuy 2003).

The distributions for each class appear unimodal with the exception of SNe Ia, whose multiple peaks were also evident in Fig. 9. These peaks suggest the existence of multiple host galaxy populations with distinct size, brightness, and morphology; additional studies have shown that SNe Ia occur within a broad range of galaxies (Gómez de Castro & Wamsteker 2006).

It is possible that these size and brightness differences between supernova host galaxies can at least in part be attributed to differences in redshift, as much struc-

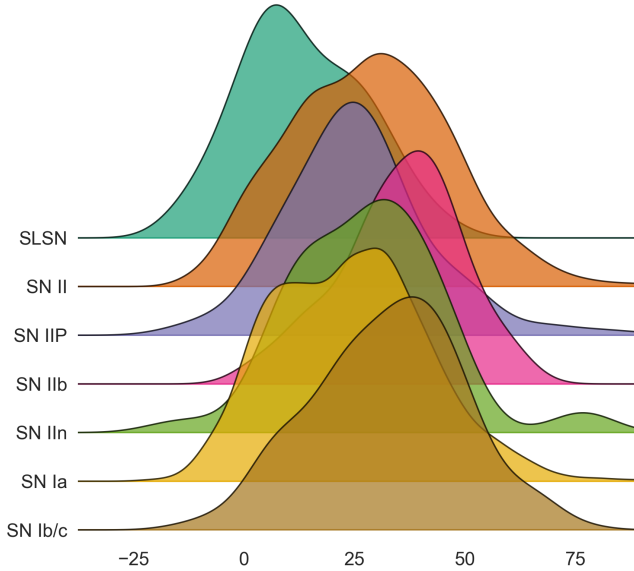


Figure 10. The distributions of supernova classes as a function of the coefficient of their projection along the first principal component from our PCA analysis. Despite strong overlap, different classes are on average associated with different host galaxy properties; in this space, a type IIb supernova (SN IIb) is easily differentiated from a superluminous supernova (SLSN).

ture information is lost for high redshift host galaxies. The fact that the postage stamp for the host galaxy at the peak of our SN Ib/c distribution reveals significantly more morphological information than the postage stamp for the host near the peak of the SLSN distribution seems to verify this prediction, as SLSNe are found at systematically higher redshifts than SNe Ib/c. In addition, the archival data we have used inevitably features a sample of supernova events at lower redshifts than is physical for that class, as the higher redshift events will not be detected. While we are unable to disentangle the host galaxy features that are redshift-dependent in our dataset from those which are not, no single magnitude-limited supernova survey to date would contain enough spectroscopically confirmed events of each class to construct a statistical sample and permit an analysis of this kind. We have found our PCA results to be consistent for a sub-sample of our data consisting of only low- z (< 0.014) host galaxies, but we caution that this work represents a first pass toward characterizing supernova host galaxies.

5. SUPERNOVA CLASSIFICATION

5.1. Random Forest: Methods

Having constructed a dataset of supernovae and the PS1 features of their associated host galaxies, we are now able to study the predictive power of this host

galaxy information for supernova classification. We implement a random forest (Breiman 2001), a supervised learning algorithm composed of an ensemble of decision trees. When used for classification, a random subset of input features is used to construct each decision tree and predict the class of a sample. This method of feature bagging allows us to estimate the importance of features by their discriminatory power across many trees. Once the trees are constructed, a final class is determined by the random forest with a majority vote of the class output at each tree. We use the random forest implementation in `sklearn`.

We first remove all host galaxy features from our final table that do not describe physically meaningful information. These include PS1 IDs, PS1 data quality flags and features that reflect the quality of model fits. We have also removed rows containing missing values, leaving 11,873 supernovae in our sample. Further, in order to enforce the accuracy of our classification data, we also drop all rows where the redshift of the associated host differs by greater than 5% from the redshift of the supernova (if both are reported). We then consolidate supernova class labels.

First, we consolidate our training data into two classes of supernovae: core collapse (including SNe Ib/c, SNe II, and all sub-classes of SN II events) and type Ia supernovae (SN Ia). The `GHOST` database contains overwhelmingly Ia supernovae, and in a magnitude-limited survey, the majority of discovered events will also be SNe Ia. Training our random forest on the observed distribution of events would improve the overall classification accuracy of our model when tested on data matching this distribution, but the tendency of the classifier to preferentially identify SNe Ia would prevent it from learning intrinsic differences between the host galaxies of under-represented supernova classes. Using the imbalanced training set would also lead to more wrong classifications for rare events, as the algorithm would determine that any event with ambiguous host galaxy properties is probably a SN Ia. Further, the intrinsic rates of under-sampled supernovae remain poorly understood (Strolger et al. 2015) and therefore poorly constrained (Prajs et al. 2017). Observed rates also suffer from known systematic effects such as Malmquist bias (Leaman et al. 2011). Without the ability to constrain the intrinsic rates of each of our supernova classes, training our model on the data directly would be teaching the model a distribution that is known to be uncharacteristic of the overall population. Because we are primarily focused in this work on characterizing host galaxies and not on maximizing classification accuracy, we re-balance our classes using the package `Imbalanced-learn`.

We first use k-fold cross-validation to generate five data samples of equal size. One of these samples is taken to be the test data in our first random forest model, and the remaining 80% of the data is used as the basis for our training set. Due to the difference in sizes between samples we decide to re-balance this training data using a mixed approach. We undersample our largest class (SN Ia) and oversample our smallest class (core collapse) to a class size in between these two extremes. This allows us to achieve a balance between training on as much data from the majority class as possible, while minimizing the amount of artificial data we generate for the minority class. After re-sampling, our distribution of training data for a single fold of the binary model contains 3,500 SN Ia events and 3,500 core collapse events. Each fold of our test set contains approximately 1,503 SN Ia events and 723 core collapse events (because our full test set is not divisible by five, each test sample will contain a slightly different number of events). The next model uses a different one of the five sub-samples for testing and the re-balanced remaining 80% of the data for training. This process is repeated for each of the five folds, generating five distinct random forests for our binary classification model. We plot pie charts describing the classes of our full dataset and our re-balanced samples in Figure 11.

We use the `RandomizedSearchCV` algorithm to determine our optimal hyperparameters for the random forest. Our final model consists of 1,400 trees without bootstrapping, and considers a maximum of 18 features (the square root of the total number of features) when choosing the best split for each node. We use a maximum depth of 90 and a minimum of 2 samples required for splitting. As with the dimensionality reduction described in §4, we scale our features to have a mean of 0 and variance of unity.

5.2. Random Forest: Results

Because the final class predicted by the model is determined by consolidating the individual predictions of each of the trees, a probability score can be calculated as the fraction of final votes belonging to each class. Traditionally, the overall accuracy in a binary classification problem is determined by the fraction of events correctly classified by a majority of trees, corresponding to a probability threshold of 0.5; however, different thresholds can be selected to prioritize different aspects of the model based on its particular application. For example, a higher probability threshold will consider only the events which are classified nearly unanimously by all of the trees, reducing the false positive rate, whereas a low probability threshold will do the opposite. This

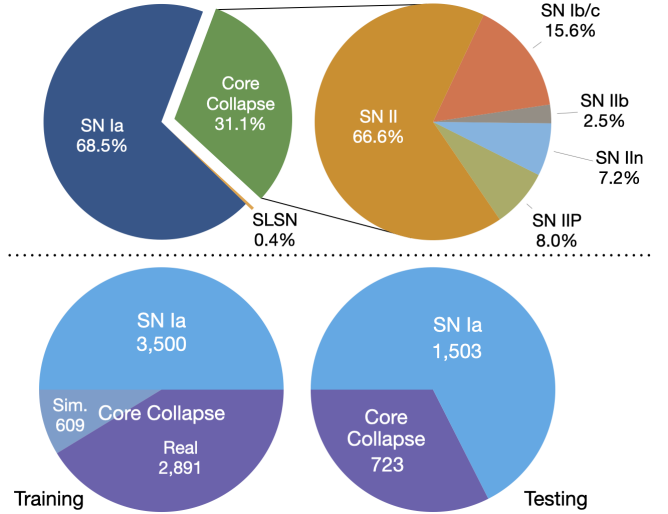


Figure 11. **Above.** The fraction of the `GHOST` database comprised by different classes of supernovae. We show the fraction of core collapse supernovae comprised by different sub-types at right. **Below.** The total number of supernovae within the training and testing samples for each fold of our two-class model. We have under-sampled our largest class (SN Ia) and over-sampled our smallest class (core collapse) to generate a balanced dataset for training our algorithm. We list the number of real and augmented core collapse events for clarity. Due to the small number of peculiar core-collapse, peculiar SN Ia, and SLSN events discovered to date, we are unable to robustly classify these groups by host galaxy properties.

tradeoff between the true positive and false positive rates can be conceptualized with a Receiver Operating Characteristic (ROC) curve, which describes the rate of true positive classifications and false positive classifications as a function of the probability threshold (from 0 to 1). The accuracy of our model determined by a majority vote represents a single point along this curve. The Area Under the ROC Curve (AUC) quantifies the separability of our two classes, with a high AUC corresponding to a model which achieves a high true positive rate and a low false positive rate. In the limit of perfect classification, with all true positive classifications and no false positives, the AUC approaches unity. We have constructed a ROC curve, given in Figure 12a, to evaluate the binary model described above. We report the AUC for each class and its sample standard deviation across our 5-folds. We also present the confusion matrix for our model in Figure 12b, which lists the mean classification accuracy (determined by a probability threshold of 0.5) for each class and for the complete test set.

We find that we can predict supernova class with $\sim 70\%$ accuracy without any spectroscopic or photometric data from the explosion itself, using exclusively host galaxy information and the angular separation between

the supernova and its galaxy. For comparison, we develop two “wishful thinking” classifiers that randomly guess the supernova type of each event, the first guessing each class 50% of the time and the second guessing “SN Ia” 100% of the time. These classifiers achieve accuracies of 50.3% and 50.0% on our re-balanced dataset, respectively, making our host galaxy classifier $\sim 20\%$ more accurate than chance. This study is the first to accurately distinguish thousands of SNe Ia and core collapse supernovae with the photometric properties of their host galaxies. The two-class model achieves an overall accuracy of $67.9\% \pm 1.7\%$, with a mean classification accuracy of 72% for SN Ia events. The AUC for our final model is $72\% \pm 2\%$ and $72\% \pm 3\%$ for SN Ia and core collapse events, respectively.

We have found across several iterations that our model accurately classifies more SNe Ia than core collapse events. Although it is possible that this is a consequence of augmenting our core collapse sample with simulated events, it is more likely that this reflects the diversity of core collapse sub-classes (SN I Ib, SN I IP, SN I Ib/c) and their host environments (Kelly & Kirshner 2012) suggested by Fig. 10. We have verified that this result is robust for a low-redshift ($z < 0.02$) subset of our database, confirming that the correlations learned by our model are not exclusively redshift-dependent.

The accuracy of the classification results applied to the binary problem suggests that host features can be used to minimize contamination within photometric samples of SNe Ia. Because these measurements will be already made by upcoming surveys, this method represents a low-overhead strategy for immediately improving cosmological studies.

We have found in section 4.1 that each of our host features does not provide unique information, so we can reduce the complexity of our classification model while sacrificing minimal accuracy. We achieve this by considering only the 13 features with high loading from Figure 9 in *grizy*. This reduces our parameter space from 317 to 65 features. We use these features to train a new random forest model, and find an accuracy for each class comparable to that reported for the full model.

Despite the differences between all seven classes in host galaxy distributions from Fig. 10, we have been unable to construct a random forest that can accurately distinguish between rarer sub-classes of supernovae, even after augmenting these classes as was done for the core collapse class. These rarer events include SLSNe, SNe IIP, SNe I Ib, and SNe I Ib/c. It is likely that there are too few of these events for our random forest to identify meaningful relationships with their host galaxies. At present, GHOST contains under 100

SLSNe. LSST in Wide-Fast-Deep mode is predicted to find $\sim 10^4$ SLSNe per year (Villar et al. 2018), dramatically expanding this dataset and facilitating future studies into the host galaxies of these smaller classes.

Because of the strong correlations between the majority of host galaxy features, the variable importances given by our random forest model may not reveal the most significant features in our model. Further, the random forest importances presented by `scikit-learn` are known to be biased⁴. For these reasons, we use the package `feature-selector` to remove all features that are greater than 80% linearly correlated and train a gradient boosting model for classification with a logloss objective function. We use the normalized feature importance, corresponding to the percentage of times the feature is used within the model, to evaluate feature significance. We list the ten most significant features from our model in Fig. 13.

The host galaxy parameters found to be most significant can be grouped into three main categories: radial offset features, including θ and θ/d_{DLR} ; color-derived features, including $4DCD$, $g-r$, $g-i$, $r-i$, and $i-z$; and morphological features, including *momentXX* in g and i and *ExtNSigma* in g . The high importance of the scaled radial offset of the supernova suggests that different classes of events trace different features of their host galaxies. The unscaled radial offset also has high importance, but this is likely a consequence of the difference in observed rates of supernova classes at different redshifts. For example, core collapse events occur in our sample predominantly at low redshift, where their observed angular offset is more likely to span a wide range of values due to the decreased distance to the host galaxy.

The morphological features characterize the light profile of the host galaxy, which can itself be an indication of the host galaxy’s morphological class on the Hubble tuning fork (van der Wel 2008). Color features encode supernova correlations with metallicity, mass, and galactic star formation rate (e.g. Hansson et al. 2012), and are also a useful discriminator of early and late-type galaxies (Strateva et al. 2001; Nair & Abraham 2010). These features suggest that similar correlations to those previously identified in literature yield the highest discriminatory power in classifying individual supernova events. The importance of host galaxy morphology measurements in classifying supernovae is further confirmed by their large loadings in PCA space from §4.1, and the color with highest importance in our random forest ($g-r$) is strongly correlated (Fig. 8) with host galaxy

⁴ <https://explained.ai/rf-importance/#intro>

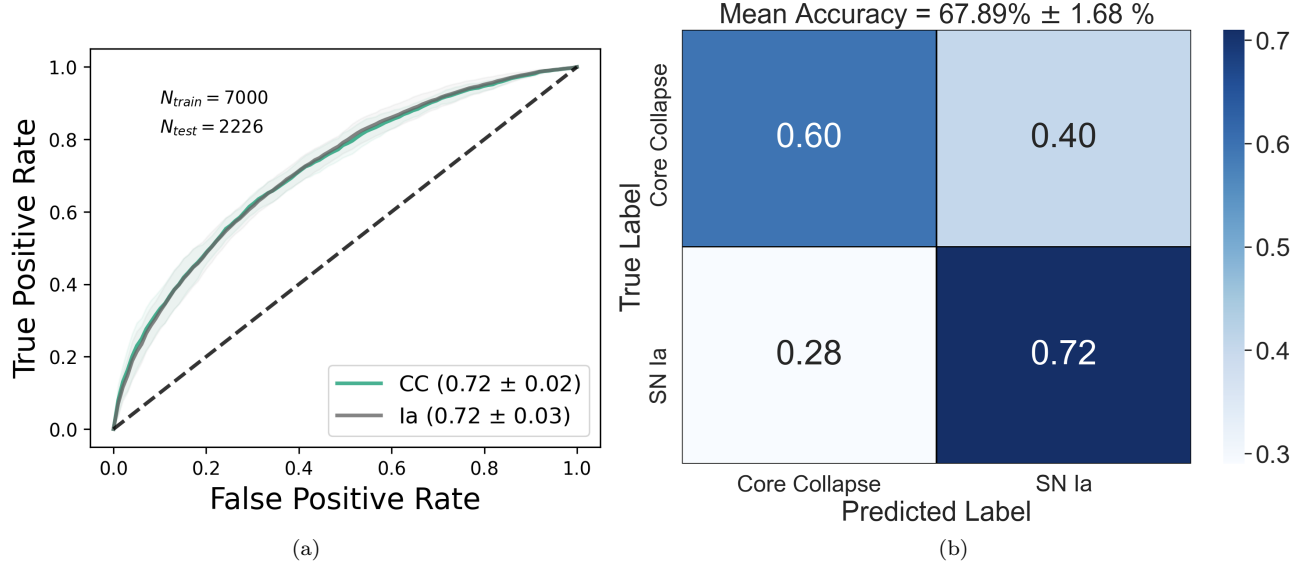


Figure 12. a. A receiver operator characteristic (ROC) curve for our random forest classifier trained to classify SNe Ia and core collapse events. Shaded regions describe the sample standard deviation calculated from a 5-fold cross-validation. The dashed line designates the performance of a model that classifies at random, and the area under the curve (AUC) for each class is listed along with its standard deviation across the 5 folds. The total number of supernovae in the training and testing sets (after augmentation) for each fold is listed top left. **b.** The confusion matrix for our classifier, showing the mean true positive rate and mean false positive rate for each class. The overall accuracy is given at top. We accurately distinguish $\sim 70\%$ of SNe Ia and core collapse events without any information from either the light curve or spectrum.

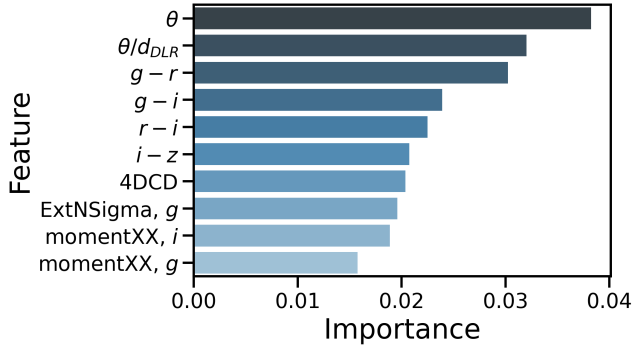


Figure 13. The ten host galaxy features with highest normalized importances determined by a gradient boosting model and ordered by importance in the binary classification model. The features with highest importance can be broadly grouped as host galaxy color, radial separation, and host galaxy light profile. All of these features are available a-priori or can be calculated immediately following a triggered event.

magnitude, another feature with strong loading in PCA space.

Foley & Mandel (2013) found that the most significant feature in increasing their FoM, which prioritized SN Ia sample purity, was host morphology. Including this data increased the FoM by greater than a factor of two over using no host galaxy information. This agrees with our finding that the features that characterize the light pro-

file of a host galaxy (ExtNSigma and $m_{\text{Ap},i} - m_{\text{Kron},i}$) are important for classification. After morphology, Foley & Mandel (2013) finds that considering host galaxy color and luminosity slightly increases their FoM and increases the spread between SN Ia and core collapse samples. While this is considered to be less significant than host galaxy morphology for maintaining pure SN Ia samples, the ability of color and luminosity to increase the separation between these two classes may explain their primary importance in the classification problem considered in this work. Finally, Foley & Mandel (2013) found that radial offset information produces only marginal contributions to SN Ia sample purities. It is surprising, then, that our random forest model uses radial offset information as its most important feature set for classification. We hypothesize that this difference can be attributed to our larger number of supernova events, which may show systematic differences in radial offset that may not be apparent in smaller samples. In addition, our core collapse sample consists of a greater number of sub-types (e.g. IIP, II_n) than were originally considered by Foley & Mandel (2013), and these sub-types may be more distinguishable by radial offset than SNe Ib/c, SNe II, and SNe Ia only.

We have additionally calculated the permutation importance of the variables in our model using the `rfpimp` package. This model identifies the top five features in our model to be $g-r$, second order moments in g and

r , $ExtNSigma$ in z and $psfMajorFWHM$ in i . These results agree with the gradient boosting features and emphasize the importance of color and derived morphological features.

Calibrated aperture flux, $psfFlux$, adaptive source intensity second moments, and their associated uncertainties will be released for each new source detected by LSST within 24 hours of detection. Difference image alerts will also present the radial offset of a transient from a likely host galaxy. From these data, comparable color, morphological, and radial features can be derived and used for transient classification. From our importances above, these measures are critical for host galaxy classification of transient events. In addition, LSST will accompany source alerts with flags to characterize the “extendedness” and “spuriousness” of detected objects, and these can be used to improve the current models for star-galaxy separation and host galaxy association, respectively. Because of the LSST baseline cadence in a single passband, these features will only be available in *ugrizy* after the first ~ 6 months of operation. During the initial period of LSST commissioning, host photometry can be retrieved from PS1.

6. SUPERNOVA SIBLINGS

By determining the host galaxies of the majority of spectroscopically confirmed supernovae, we can compare the properties of supernova siblings - that is, supernovae associated with a single host galaxy. Extensive work has been done to compare the light curves of SN Ia siblings (Gall et al. 2018; Scolnic et al. 2020) and conduct a census of supernova siblings (Guthrie 1990; Anderson & Soto 2013). We find that 304 galaxies in our sample host 2 supernovae, 37 galaxies host 3 supernovae, 5 host 4 supernovae, 4 host 5 supernovae and 3 host 6 supernovae. These are nearly half of the supernova siblings identified by <http://www.rochesterastronomy.org/snimages/sndupe.html>. The majority of missing pairs were dropped from our pipeline because a supernova was located greater than $30''$ from its host galaxy center, as is the case for low- z host galaxies; however, increasing our cone search would have increased the number of artifacts labeled as potential host galaxies and decreased the accuracy of our matches.

For the siblings we have identified, we use the radial offset θ to explore whether SNe II and SNe Ia probe distinct regions of their host galaxy. For all galaxies hosting multiple supernovae, we take the difference between the radial offsets of the first two supernova siblings, $\delta\theta$. We then estimate the probability density function of these values with KDEs for siblings of the same class, where both siblings are SNe II or both are SNe Ia (the matched

sample), and for siblings of different classes, with one sibling as SN Ia and the other as SN II (the nonmatched sample). These two samples sizes are roughly equal. Because we are comparing the *difference* in θ between matched and nonmatched supernova siblings, we minimize the influence of different galaxy sizes, distances, and redshifts. A Malmquist bias is present within this sample, as supernovae within nearby host galaxies will be more easily detected than distant supernovae, especially for SNe II. These host galaxies allow for a greater range of possible $\delta\theta$ values than distant galaxies, so a SN II/SN II match will likely have a larger relative separation than a SN Ia/SN Ia match. This effect is unlikely to mask a systematic difference between $\delta\theta$ for matched and unmatched siblings.

We perform an Anderson-Darling (AD) test to compare the distributions of θ for matched and unmatched supernovae, and find that at $> 99.8\%$ confidence we can reject the null hypothesis that these two samples are drawn from the same distribution ($p = 0.002$). A Kolmogorov-Smirnov (KS) test, which weights the distribution tails less heavily than the AD test, also finds a significant difference between these distributions at the 99% level ($p = 0.01$).

Wang et al. (1997) makes a similar comparison between the radial offsets (in kpc) of 197 SNe II and 246 SNe Ia using a KS test, rejecting the null hypothesis that these two classes have the same radial distributions at $p = 10\%$ (or at the 90% confidence level). Wang et al. (1997) further suggests that the dominant differences between the radial offsets of these two classes arise within the inner 6 kpc of a galaxy. To compare the inner radial distributions of the two classes between galaxies, we can no longer use $\delta\theta$; instead, we compare the scaled radial offset values θ/d_{DLR} for SNe Ia and SNe II for our entire GHOST dataset. We find no significant difference in θ/d_{DLR} between SNe Ia and SNe II, either in the full range of values ($p = 0.47$ for KS and $p > 0.25$ for AD) or within the inner 10% of a supernova’s host galaxy ($p = 0.57$ for KS and $p > 0.25$ for AD). We have found this result to be consistent for the low- z sample ($z < 0.014$). We caution that we have calculated the DLR for these galaxies using the Kron radius reported for these objects; If this radius is not representative of the true radius of the galaxy, it would decrease the robustness of this comparison.

7. COMPARING HOST GALAXY DISTRIBUTIONS WITH TSNE

While PCA is useful for visualizing data, it is only able to compose reduced dimensional spaces from linear combinations of features, evident in the wide separa-

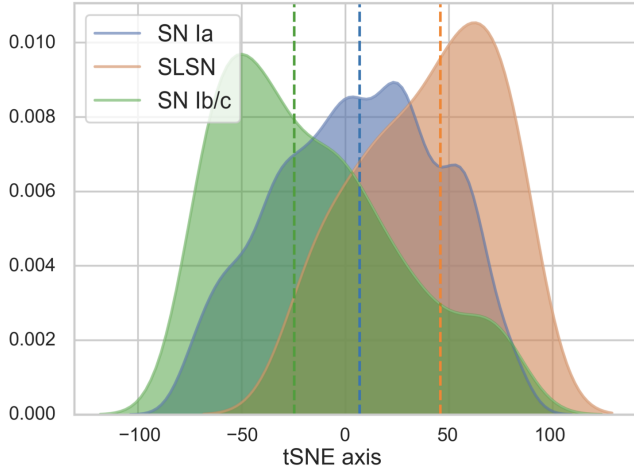


Figure 14. Host galaxy feature KDEs for SNe Ia, SNe Ib/c, and SLSNe along the first dimension of our 2D tSNE, with dashed lines indicating the median of each distribution. Relative positions and shapes of the three distributions are consistent with the results from our principal component analysis given in 10, suggesting different underlying galaxy populations.

ration between host galaxy magnitude and flux in Fig. 9. To explore nonlinear relationships between our host galaxy features, we implement t-Distributed Stochastic Neighbor Embedding (tSNE) (van der Maaten & Hinton 2008). In tSNE, the transformation preserves the distribution of separations between points. This makes it another useful tool for directly comparing multiple classes of objects.

We begin by projecting our data into a three-dimensional tSNE space using the `sklearn` implementation, using a perplexity of 30 and a learning rate of 200. To compare with our PCA results in Figure 10, we project our supernovae along only the first tSNE axis. We present KDEs for our transformed host galaxy data for SNe Ia, SNe Ib/c, and SLSNe along this axis in Fig. 14. As before, we see a leftward skew for SLSN host galaxies and rightward skew for SN Ib/c host galaxies. The medians of these distributions occur at significantly different positions along this tSNE axis. tSNE is a stochastic algorithm, and we have verified through multiple runs that the differences between our distributions are insensitive to the random seed used. These results suggest that the systematic differences between core collapse, SN Ia, and SLSN host galaxies are robust, with SLSNe preferentially found in small and faint host galaxies and core collapse supernovae found preferentially in large, bright host galaxies where specific star formation is high.

To further explore nonlinear correlations, we then plot our supernova host galaxy features in the full three-

dimensional t-SNE space. We find striking visual differences in the distributions of SN IIP, SLSN, and SN IIB host galaxy features along the second and third t-SNE axes, which we plot in Fig. 15. SLSN and SN IIB host galaxies are most easily distinguished in this space, and SN IIP hosts are centered near the middle of the two distributions and span the full space of SN host galaxy features. We have found the separation between SN IIB and SLSN host galaxies to be robust for a range of perplexities and initial random seeds, suggesting that real discriminatory information exists between these classes. These results also suggest that certain supernova sub-types may be even easier to distinguish using host galaxy features than SNe Ia and core collapse events. Once more of these events are discovered with LSST, future work should be devoted to classifying these events from the rich host galaxy information collected.

As we have mentioned before, it is likely that the photometric differences between host galaxies that we have identified in this work are in part consequences of the difference in redshift-dependent observations for each class of supernovae. This relationship becomes evident when we plot the redshifts for the same SN IIP, SN IIB, and SLSN host galaxies described above. In Figure 7, we find that redshift roughly decreases along the positive horizontal tSNE axis and along the negative vertical tSNE axis. This result reflects previous findings that SLSNe preferentially occur at high- z and core collapse events have been preferentially observed at low- z , particularly SNe IIB (Kelly & Kirshner 2012). Without redshift-corrected photometry, these systematic and rate effects will obfuscate intrinsic differences between host galaxies; nevertheless, this trend can be leveraged to validate rates of each class within simulated datasets. This same validation can be applied in reverse, where a classification derived from spectral follow-up can inform photometric redshifts estimates for the supernova’s host galaxy.

8. DISCUSSION

We have constructed the largest catalogue to date of supernovae and their host galaxies. By combining the DLR method with a gradient ascent algorithm based on the light profiles of nearby sources, we are able to associate host galaxies spanning a wide range of redshifts ($0.00015 \leq z \leq 2$) to an accuracy of $> 97\%$. Upcoming surveys will image the sky to unprecedented depths; LSST will have a maximum all-band wide-field-deep depth of $5\sigma > 25.08$, and the Nancy Grace Roman Space Telescope in deep survey mode is slated to achieve a depth per exposure of 26.2 in J and H (Hounsell et al. 2018). This will allow us to study supernova

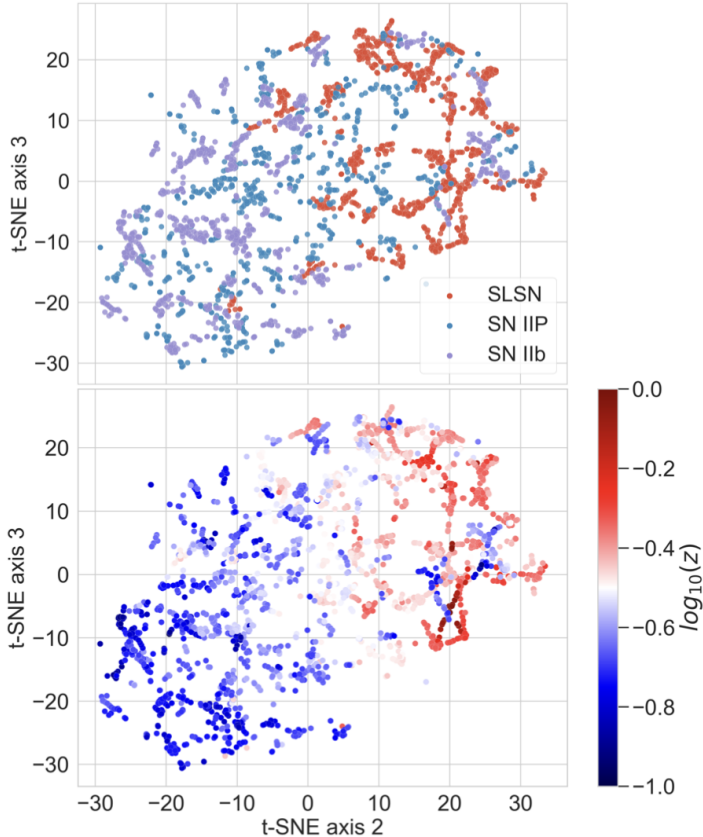


Figure 15. *Above.* The distribution of host features corresponding to three classes of supernovae (SNe IIP, SNe IIB, and SLSNe) along our second and third tSNE axes. SLSN and SN IIB host galaxies are easily separable in this space, whereas SN IIP hosts are centered between the two distributions and span a much wider range of values. *Below.* The same host galaxies as above, colored by redshift. The clustering of SNe IIB and SLSNe in tSNE space is highly redshift-dependent.

host galaxies in unprecedented detail and further explore the correlations between host galaxy and transient, but it will also exacerbate the issues described in §2.4 affecting host galaxy associations made using the DLR method. A light profile-based association method will allow us to leverage the strengths of these surveys and continue to accurately associate new transient events.

Our results indicate that contextual information can aid in supernova classification. By projecting our host galaxy information into reduced parameter spaces, we can immediately identify visual differences between supernova host galaxies. Using a random forest classifier, we can distinguish SNe Ia and core-collapse supernovae with $\sim 70\%$ accuracy using host galaxy information from PS1 alone. This work builds on previous efforts by incorporating a significantly larger number of host

galaxy features than were considered by Foley & Mandel (2013).

We find our host galaxy features with the most discriminatory power in supernova classification to be radial offset, color, and derived morphological features. The color and morphology features capture galaxy-averaged correlations with supernovae that have been previously identified in literature, and reflect the need for accurate morphological estimates in large surveys. Further, the importance of radial offset suggests that local galactic environment may be even more predictive of supernova class than the galaxy-averaged features. The strong overlap between global features of SN Ia, SLSN, and SN Ib/c host galaxies in Fig. 9 reinforces this need for localized metrics to characterize the environments of supernovae and more accurately distinguish supernova type.

In addition, we find a statistically significant difference between the differential radial offsets $\delta\theta$ of matched (SN Ia, SN Ia and SN II, SN II) and nonmatched (SN Ia, SN II) supernova siblings, but we do not find a significant difference in the scaled radial offsets θ/d_{DLR} between SNe Ia and SNe II. Intuitively, one might expect these two distributions to differ for core collapse supernovae with star-forming regions, which are more likely to be found in the arms of spiral galaxies. Our result suggests that angular offset alone may not sufficiently characterize the positions of star forming regions. In addition, the significance of radial offset in our binary classification suggests that sub-types of core collapse events (SNe IIP, SNe Ib/c, SNe IIn) may differ from SNe Ia in radial offset even if SNe II may not. This result underscores the need for higher resolution imaging to assemble a more complete picture of supernova and host galaxy interactions at the local level, which can influence both supernova class and cosmologically relevant light curve features of SNe Ia. This result may also reflect the limitations of characterizing host galaxy morphology using the Kron radius. We have found this value to be unphysical or unreported for the the largest and smallest host galaxies of our sample, limiting our ability to directly compare SN positions between galaxies.

LSST’s dedicated strategy for host galaxy association has yet to be determined. We have shown that, where deep surveys limit the ability to de-blend extended sources, the directional light radius is unable to robustly identify supernova host galaxies. In addition, the postage stamps associated with real-time transient alerts for LSST are unlikely to exceed $6'' \times 6''$. This window will exclude many supernova host galaxies within

$z \sim 0.1$ (See Figure 6a), and make it difficult to leverage postage stamp gradients for host galaxy association. The gradient ascent method outlined in this work will be a valuable resource for validating LSST’s real-time host galaxy associations and proposing improvements to the pipeline.

By identifying these features now, we will inform the development of brokers for the LSST Dark Energy Science Collaboration (DESC), which will perform initial alert prioritization and photometric classification on the full LSST alert stream. These brokers will need to perform low-latency, accurate classification of transient events using the information provided by the real-time alerts stream. For LSST, these alert packets will include the supernova radial offset, a photometric redshift, and a postage stamp of the field. After using this information to verify the host galaxy, the broker can retrieve archival LSST (or PS1, if it is not available) photometry for that host galaxy, calculate the color of the host, and use the random forest model described above to predict the class of the supernova. When combined with a real-time photometric classifier such as RAPID (Muthukrishna et al. 2019), we can ensure accurate classification pre-maximum for a broad range of transient events.

9. FUTURE WORK

The GHOST database will be valuable for future studies into the correlations between supernovae and their host galaxies. A strong correlation has been identified between local stellar mass and distance residuals for low- z Ias, corrections for which would reduce the uncertainties placed on H_0 (Jones et al. 2018b); further, a local color step derived from 2MASS photometry of a sample of Type Ia supernovae was found to be significant to 7σ (Roman et al. 2018), with a similarly significant (5.7σ) correlation identified as a function of local specific star formation rate (Rigault et al. 2018). The LSST DESC Science Roadmap lists a vital collaboration goal as identifying the underlying physics of the SN-host galaxy mass correlation for cosmological analysis. Our database contains $> 9,200$ SNe Ia, and by increasing the sample size of associated SNe Ia by at least an order of magnitude (compared to e.g. Sako et al. 2018) this data will shed more light on this connection.

Our tSNE results suggest there are systematic differences in the host galaxies of supernova sub-types that we have not yet incorporated into a classification model. These redshift-dependent differences may not be significant enough for accurate classification by themselves, but are likely to improve the accuracy of photometric classifiers. We will explore this possibility when devel-

oping an ensemble host photometry-SN photometry ensemble classifier in the future.

In addition, we will continue improving our gradient ascent algorithm. We have avoided incorporating spectroscopic redshift information into this algorithm so that the method may be automated on the alert streams of large surveys, but it is likely that knowledge of a photo- z would inform both the use of the method over DLR and the selection of a relevant step size for the field. An accurate pipeline for host galaxy association will enable discoveries across a broad range of time-domain studies, such as by constraining kilonova progenitor models (Jiang et al. 2020) verifying the discovery of Tidal Disruption Events (Arcavi et al. 2016), and further uncovering the relationship between Rapidly Evolving Transients (RETs) and their host galaxies (Wiseman et al. 2020).

We will next explore the use of Convolutional Neural Networks (CNNs) to classify supernovae using postage stamps of their host galaxies. Postage stamps encode rich, spatially resolved color and brightness information that will be critical for transient classification over the single-statistic PS1 summary features we have considered here, such as through measurements of radial color gradients (Park & Choi 2005). CNNs have shown early success in binary classification (SN Ia vs not SN Ia) of simulated supernovae (Kimura et al. 2017), and GHOST represents an ideal sample for extending this work. Host galaxy-transient correlations are also critical for plausibly embedding supernovae into postage stamps for training photometric classifiers, another primary goal for LSST DESC. By extracting these host galaxy features directly from image data, we will be able to more accurately encode these correlations into our simulations.

10. ACKNOWLEDGEMENTS

Author contributions are listed below.

A. Gagliano: Software, website, and database development; writing and editing.
 G. Narayan: Oversight, writing and editing.
 A. Engel: Contributed software for classifier.
 M. Carrasco-Kind: Contributed software for the GHOST Viewer.

This paper has undergone internal review in the LSST Dark Energy Science Collaboration. The internal reviewers were Ryan Foley, Renee Hlozek, Kaisey Mandel, Christian Setzer, and Seth Digel. The authors thank the internal reviewers for their detailed comments of this work, as they significantly strengthened this paper.

The DESC acknowledges ongoing support from the Institut National de Physique Nucléaire et de Physique

des Particules in France; the Science & Technology Facilities Council in the United Kingdom; and the Department of Energy, the National Science Foundation, and the LSST Corporation in the United States. DESC uses resources of the IN2P3 Computing Center (CC-IN2P3–Lyon/Villeurbanne - France) funded by the Centre National de la Recherche Scientifique; the National Energy Research Scientific Computing Center, a DOE Office of Science User Facility supported by the Office of Science of the U.S. Department of Energy under Contract No. DE-AC02-05CH11231; STFC DiRAC HPC Facilities, funded by UK BIS National E-infrastructure capital grants; and the UK particle physics grid, supported by the GridPP Collaboration. This work was performed in part under DOE Contract DE-AC02-76SF00515.

AG is supported by the Illinois Distinguished Fellowship, the NSF Graduate Research Fellowship, and the Center for Astrophysical Surveys Graduate Fellowship at the University of Illinois. GN’s work on this project was partially supported by the Lasker Data Science Fellowship at STScI, and generous startup funding from the University of Illinois. The authors thank the Space Telescope Science Institute for providing travel funds for AG. We are also grateful for the support of the National Center for Supercomputing Applications (NCSA), which houses the server that runs the `GHOST` database. The authors thank Rahul Biswas, Qinan Wang and Monika Soraisam for fruitful conversations related to this work.

The Pan-STARRS1 Surveys (PS1) and the PS1 public science archive have been made possible through contributions by the Institute for Astronomy, the University of Hawaii, the Pan-STARRS Project Office, the Max-Planck Society and its participating institutes, the Max Planck Institute for Astronomy, Heidelberg and the Max Planck Institute for Extraterrestrial Physics, Garching, The Johns Hopkins University, Durham University, the University of Edinburgh, the Queen’s University Belfast, the Harvard-Smithsonian Center for Astrophysics, the Las Cumbres Observatory Global Telescope Network Incorporated, the National Central University of Taiwan, the Space Telescope Science Institute, the National Aeronautics and Space Administration under Grant No. NNX08AR22G issued through the Planetary Science Di-

vision of the NASA Science Mission Directorate, the National Science Foundation Grant No. AST-1238877, the University of Maryland, Eotvos Lorand University (ELTE), the Los Alamos National Laboratory, and the Gordon and Betty Moore Foundation.

Funding for the Sloan Digital Sky Survey IV has been provided by the Alfred P. Sloan Foundation, the U.S. Department of Energy Office of Science, and the Participating Institutions. SDSS-IV acknowledges support and resources from the Center for High-Performance Computing at the University of Utah. The SDSS web site is www.sdss.org. SDSS-IV is managed by the Astrophysical Research Consortium for the Participating Institutions of the SDSS Collaboration including the Brazilian Participation Group, the Carnegie Institution for Science, Carnegie Mellon University, the Chilean Participation Group, the French Participation Group, Harvard-Smithsonian Center for Astrophysics, Instituto de Astrofísica de Canarias, The Johns Hopkins University, Kavli Institute for the Physics and Mathematics of the Universe (IPMU) / University of Tokyo, the Korean Participation Group, Lawrence Berkeley National Laboratory, Leibniz Institut für Astrophysik Potsdam (AIP), Max-Planck-Institut für Astronomie (MPIA Heidelberg), Max-Planck-Institut für Astrophysik (MPA Garching), Max-Planck-Institut für Extraterrestrische Physik (MPE), National Astronomical Observatories of China, New Mexico State University, New York University, University of Notre Dame, Observatório Nacional / MCTI, The Ohio State University, Pennsylvania State University, Shanghai Astronomical Observatory, United Kingdom Participation Group, Universidad Nacional Autónoma de México, University of Arizona, University of Colorado Boulder, University of Oxford, University of Portsmouth, University of Utah, University of Virginia, University of Washington, University of Wisconsin, Vanderbilt University, and Yale University.

This research has made use of the following Python software packages: `Astropy` (Price-Whelan et al. 2018), `Matplotlib` (Hunter 2007), `Pandas` (McKinney et al. 2010), `NumPy` (van der Walt et al. 2011), `Seaborn` (Waskom et al. 2014), `SciPy` (Virtanen et al. 2020), `Scikit-Learn` (Pedregosa et al. 2012), and `Imbalanced-learn` (Lemaître et al. 2017).

REFERENCES

- Anderson, J. P., & Soto, M. 2013, *A&A*, 550, A69, doi: [10.1051/0004-6361/201220600](https://doi.org/10.1051/0004-6361/201220600)
- Angus, C. R., Levan, A. J., Perley, D. A., et al. 2016, *MNRAS*, 458, 84, doi: [10.1093/mnras/stw063](https://doi.org/10.1093/mnras/stw063)
- Arcavi, I., French, K. D., & Zabludoff, A. I. 2016, 228, 314-02
- Baldeschi, A., Miller, A., Stroh, M., Margutti, R., & Coppejans, D. L. 2020, arXiv e-prints, arXiv:2005.00155. <https://arxiv.org/abs/2005.00155>

- Bell, E. F., Wolf, C., Meisenheimer, K., et al. 2004, *ApJ*, 608, 752, doi: [10.1086/420778](https://doi.org/10.1086/420778)
- Breiman, L. 2001, *Machine learning*, 45, 5
- Cappellaro, E., Evans, R., & Turatto, M. 1999, *A&A*, 351, 459. <https://arxiv.org/abs/astro-ph/9904225>
- Chambers, K. C., Magnier, E. A., Metcalfe, N., et al. 2016, *arXiv e-prints*, arXiv:1612.05560. <https://arxiv.org/abs/1612.05560>
- Cooke, J., Sullivan, M., Gal-Yam, A., et al. 2012, *Nature*, 491, 228, doi: [10.1038/nature11521](https://doi.org/10.1038/nature11521)
- Cortes, C., & Vapnik, V. 1995, *Machine learning*, 20, 273
- Corwin, Harold G., J., Buta, R. J., & de Vaucouleurs, G. 1994, *AJ*, 108, 2128, doi: [10.1086/117225](https://doi.org/10.1086/117225)
- Covey, K. R., Ivezić, Ž., Schlegel, D., et al. 2007, *AJ*, 134, 2398, doi: [10.1086/522052](https://doi.org/10.1086/522052)
- D’Andrea, C. B., Gupta, R. R., Sako, M., et al. 2011, *ApJ*, 743, 172, doi: [10.1088/0004-637X/743/2/172](https://doi.org/10.1088/0004-637X/743/2/172)
- De, K., Kasliwal, M. M., Polin, A., et al. 2019, *ApJL*, 873, L18, doi: [10.3847/2041-8213/ab0aec](https://doi.org/10.3847/2041-8213/ab0aec)
- Dimitriadis, G., Foley, R. J., Rest, A., et al. 2019, *ApJL*, 870, L1, doi: [10.3847/2041-8213/aadbb0](https://doi.org/10.3847/2041-8213/aadbb0)
- Dressler, A., Lynden-Bell, D., Burstein, D., et al. 1987, *ApJ*, 313, 42, doi: [10.1086/164947](https://doi.org/10.1086/164947)
- Ferretti, R., Amanullah, R., Goobar, A., et al. 2017, *A&A*, 606, A111, doi: [10.1051/0004-6361/201731409](https://doi.org/10.1051/0004-6361/201731409)
- Foley, R. J., & Mandel, K. 2013, *ApJ*, 778, 167, doi: [10.1088/0004-637X/778/2/167](https://doi.org/10.1088/0004-637X/778/2/167)
- Foley, R. J., Scolnic, D., Rest, A., et al. 2018, *MNRAS*, 475, 193, doi: [10.1093/mnras/stx3136](https://doi.org/10.1093/mnras/stx3136)
- Galbany, L., Miquel, R., Östman, L., et al. 2012, *ApJ*, 755, 125, doi: [10.1088/0004-637X/755/2/125](https://doi.org/10.1088/0004-637X/755/2/125)
- Gall, C., Stritzinger, M. D., Ashall, C., et al. 2018, *A&A*, 611, A58, doi: [10.1051/0004-6361/201730886](https://doi.org/10.1051/0004-6361/201730886)
- Gómez de Castro, A. I., & Wamsteker, W. 2006, *Fundamental Questions in Astrophysics: Guidelines for Future UV Observatories*, Vol. 303
- Gupta, R. R. 2013, *Publicly Accessible Penn Dissertations*, 758
- Gupta, R. R., Kuhlmann, S., Kovacs, E., et al. 2016, *AJ*, 152, 154, doi: [10.3847/0004-6256/152/6/154](https://doi.org/10.3847/0004-6256/152/6/154)
- Guthrie, B. N. G. 1990, *A&A*, 234, 84
- Hakobyan, A. A., Nazaryan, T. A., Adibekyan, V. Z., et al. 2014, *MNRAS*, 444, 2428, doi: [10.1093/mnras/stu1598](https://doi.org/10.1093/mnras/stu1598)
- Hamuy, M. 2003, *ApJ*, 582, 905, doi: [10.1086/344689](https://doi.org/10.1086/344689)
- Hamuy, M., Phillips, M. M., Suntzeff, N. B., et al. 1996, *AJ*, 112, 2391, doi: [10.1086/118190](https://doi.org/10.1086/118190)
- Hansson, K. S. A., Lisker, T., & Grebel, E. K. 2012, *MNRAS*, 427, 2376, doi: [10.1111/j.1365-2966.2012.21659.x](https://doi.org/10.1111/j.1365-2966.2012.21659.x)
- Henne, V., Pruzhinskaya, M. V., Rosnet, P., et al. 2017, *NewA*, 51, 43, doi: [10.1016/j.newast.2016.08.009](https://doi.org/10.1016/j.newast.2016.08.009)
- High, F. W., Stubbs, C. W., Rest, A., Stalder, B., & Challis, P. 2009, *AJ*, 138, 110, doi: [10.1088/0004-6256/138/1/110](https://doi.org/10.1088/0004-6256/138/1/110)
- Höflich, P., Krisciunas, K., Khokhlov, A. M., et al. 2010, *ApJ*, 710, 444, doi: [10.1088/0004-637X/710/1/444](https://doi.org/10.1088/0004-637X/710/1/444)
- Hosseinzadeh, G., Sand, D. J., Valenti, S., et al. 2017, *ApJL*, 845, L11, doi: [10.3847/2041-8213/aa8402](https://doi.org/10.3847/2041-8213/aa8402)
- Hounsell, R., Scolnic, D., Foley, R. J., et al. 2018, *ApJ*, 867, 23, doi: [10.3847/1538-4357/aac08b](https://doi.org/10.3847/1538-4357/aac08b)
- Hunter, J. D. 2007, *Computing in Science and Engineering*, 9, 90, doi: [10.1109/MCSE.2007.55](https://doi.org/10.1109/MCSE.2007.55)
- Ishida, E. E. O., & de Souza, R. S. 2013, *MNRAS*, 430, 509, doi: [10.1093/mnras/sts650](https://doi.org/10.1093/mnras/sts650)
- Ivezić, Ž., Kahn, S. M., Tyson, J. A., et al. 2019, *ApJ*, 873, 111, doi: [10.3847/1538-4357/ab042c](https://doi.org/10.3847/1538-4357/ab042c)
- Jiang, J.-A., Doi, M., Maeda, K., et al. 2017, *Nature*, 550, 80, doi: [10.1038/nature23908](https://doi.org/10.1038/nature23908)
- Jiang, Z., Wang, J., Zhang, F., et al. 2020, *MNRAS*, doi: [10.1093/mnras/staa1989](https://doi.org/10.1093/mnras/staa1989)
- Jones, D. O., Scolnic, D. M., Riess, A. G., et al. 2018a, *ApJ*, 857, 51, doi: [10.3847/1538-4357/aab6b1](https://doi.org/10.3847/1538-4357/aab6b1)
- Jones, D. O., Riess, A. G., Scolnic, D. M., et al. 2018b, *ApJ*, 867, 108, doi: [10.3847/1538-4357/aae2b9](https://doi.org/10.3847/1538-4357/aae2b9)
- Jones, D. O., French, K. D., Agnello, A., et al. 2019, *Transient Name Server AstroNote*, 148, 1
- . 2020, in prep.
- Karpenka, N. V., Feroz, F., & Hobson, M. P. 2013, *MNRAS*, 429, 1278, doi: [10.1093/mnras/sts412](https://doi.org/10.1093/mnras/sts412)
- Kelly, P. L., Filippenko, A. V., Modjaz, M., & Kocevski, D. 2014, *ApJ*, 789, 23, doi: [10.1088/0004-637X/789/1/23](https://doi.org/10.1088/0004-637X/789/1/23)
- Kelly, P. L., Hicken, M., Burke, D. L., Mandel, K. S., & Kirshner, R. P. 2010, *ApJ*, 715, 743, doi: [10.1088/0004-637X/715/2/743](https://doi.org/10.1088/0004-637X/715/2/743)
- Kelly, P. L., & Kirshner, R. P. 2012, *ApJ*, 759, 107, doi: [10.1088/0004-637X/759/2/107](https://doi.org/10.1088/0004-637X/759/2/107)
- Kessler, R., Conley, A., Jha, S., & Kuhlmann, S. 2010, *arXiv e-prints*, arXiv:1001.5210. <https://arxiv.org/abs/1001.5210>
- Kessler, R., Narayan, G., Avelino, A., et al. 2019, *PASP*, 131, 094501, doi: [10.1088/1538-3873/ab26f1](https://doi.org/10.1088/1538-3873/ab26f1)
- Kim, A. G., Aldering, G., Antilogus, P., et al. 2014, *ApJ*, 784, 51, doi: [10.1088/0004-637X/784/1/51](https://doi.org/10.1088/0004-637X/784/1/51)
- Kimura, A., Takahashi, I., Tanaka, M., et al. 2017, *arXiv e-prints*, arXiv:1711.11526. <https://arxiv.org/abs/1711.11526>
- Kulkarni, S. R., Perley, D. A., & Miller, A. A. 2018, *ApJ*, 860, 22, doi: [10.3847/1538-4357/aabf85](https://doi.org/10.3847/1538-4357/aabf85)

- Lampeitl, H., Smith, M., Nichol, R. C., et al. 2010, *ApJ*, 722, 566, doi: [10.1088/0004-637X/722/1/566](https://doi.org/10.1088/0004-637X/722/1/566)
- Leaman, J., Li, W., Chornock, R., & Filippenko, A. V. 2011, *MNRAS*, 412, 1419, doi: [10.1111/j.1365-2966.2011.18158.x](https://doi.org/10.1111/j.1365-2966.2011.18158.x)
- Leloudas, G., Schulze, S., Krühler, T., et al. 2015, *MNRAS*, 449, 917, doi: [10.1093/mnras/stv320](https://doi.org/10.1093/mnras/stv320)
- Lemaître, G., Nogueira, F., & Aridas, C. K. 2017, *Journal of Machine Learning Research*, 18, 1, <http://jmlr.org/papers/v18/16-365.html>
- Lochner, M., McEwen, J. D., Peiris, H. V., Lahav, O., & Winter, M. K. 2016, *ApJS*, 225, 31, doi: [10.3847/0067-0049/225/2/31](https://doi.org/10.3847/0067-0049/225/2/31)
- Lunnan, R., Chornock, R., Berger, E., et al. 2015, *ApJ*, 804, 90, doi: [10.1088/0004-637X/804/2/90](https://doi.org/10.1088/0004-637X/804/2/90)
- Magnier, E. A., Sweeney, W. E., Chambers, K. C., et al. 2016, *arXiv e-prints*, arXiv:1612.05244, <https://arxiv.org/abs/1612.05244>
- Mandel, K. S., Scolnic, D. M., Shariff, H., Foley, R. J., & Kirshner, R. P. 2017, *ApJ*, 842, 93, doi: [10.3847/1538-4357/aa6038](https://doi.org/10.3847/1538-4357/aa6038)
- McKinney, W., et al. 2010, in *Proceedings of the 9th Python in Science Conference*, Vol. 445, Austin, TX, 51–56
- Miller, A. A., Magee, M. R., Polin, A., et al. 2020, *arXiv e-prints*, arXiv:2005.05972, <https://arxiv.org/abs/2005.05972>
- Möller, A., & de Boissière, T. 2020, *MNRAS*, 491, 4277, doi: [10.1093/mnras/stz3312](https://doi.org/10.1093/mnras/stz3312)
- Muthukrishna, D., Narayan, G., Mandel, K. S., Biswas, R., & Hložek, R. 2019, *PASP*, 131, 118002, doi: [10.1088/1538-3873/ab1609](https://doi.org/10.1088/1538-3873/ab1609)
- Nair, P. B., & Abraham, R. G. 2010, *ApJS*, 186, 427, doi: [10.1088/0067-0049/186/2/427](https://doi.org/10.1088/0067-0049/186/2/427)
- Narayan, G., Zaidi, T., Soraisam, M. D., et al. 2018, *ApJS*, 236, 9, doi: [10.3847/1538-4365/aab781](https://doi.org/10.3847/1538-4365/aab781)
- Nicholl, M., Blanchard, P. K., Berger, E., et al. 2020, *Nature Astronomy*, doi: [10.1038/s41550-020-1066-7](https://doi.org/10.1038/s41550-020-1066-7)
- Oemler, A., J., & Tinsley, B. M. 1979, *AJ*, 84, 985, doi: [10.1086/112502](https://doi.org/10.1086/112502)
- Park, C., & Choi, Y.-Y. 2005, *ApJL*, 635, L29, doi: [10.1086/499243](https://doi.org/10.1086/499243)
- Pedregosa, F., Varoquaux, G., Gramfort, A., et al. 2012, *arXiv e-prints*, arXiv:1201.0490, <https://arxiv.org/abs/1201.0490>
- Perley, D. A., Quimby, R. M., Yan, L., et al. 2016, *ApJ*, 830, 13, doi: [10.3847/0004-637X/830/1/13](https://doi.org/10.3847/0004-637X/830/1/13)
- Perlmutter, S., Aldering, G., Goldhaber, G., et al. 1999, *ApJ*, 517, 565, doi: [10.1086/307221](https://doi.org/10.1086/307221)
- Poznanski, D., Maoz, D., & Gal-Yam, A. 2007, *AJ*, 134, 1285, doi: [10.1086/520956](https://doi.org/10.1086/520956)
- Poznanski, D., Chornock, R., Nugent, P. E., et al. 2010, *Science*, 327, 58, doi: [10.1126/science.1181709](https://doi.org/10.1126/science.1181709)
- Prajs, S., Sullivan, M., Smith, M., et al. 2017, *MNRAS*, 464, 3568, doi: [10.1093/mnras/stw1942](https://doi.org/10.1093/mnras/stw1942)
- Prentice, S. J., Maguire, K., Smartt, S. J., et al. 2018, *ApJL*, 865, L3, doi: [10.3847/2041-8213/aadd90](https://doi.org/10.3847/2041-8213/aadd90)
- Price-Whelan, A. M., Sipőcz, B. M., Günther, H. M., et al. 2018, *AJ*, 156, 123
- Rest, A., Garnavich, P. M., Khatami, D., et al. 2018, *Nature Astronomy*, 2, 307, doi: [10.1038/s41550-018-0423-2](https://doi.org/10.1038/s41550-018-0423-2)
- Riess, A. G., Filippenko, A. V., Challis, P., et al. 1998, *AJ*, 116, 1009, doi: [10.1086/300499](https://doi.org/10.1086/300499)
- Rigault, M., Brinnel, V., Aldering, G., et al. 2018, *arXiv e-prints*, arXiv:1806.03849, <https://arxiv.org/abs/1806.03849>
- Roman, M., Hardin, D., Betoule, M., et al. 2018, *A&A*, 615, A68, doi: [10.1051/0004-6361/201731425](https://doi.org/10.1051/0004-6361/201731425)
- Sako, M., Bassett, B., Becker, A. C., et al. 2018, *PASP*, 130, 064002, doi: [10.1088/1538-3873/aab4e0](https://doi.org/10.1088/1538-3873/aab4e0)
- Schlafly, E. F., & Finkbeiner, D. P. 2011, *ApJ*, 737, 103, doi: [10.1088/0004-637X/737/2/103](https://doi.org/10.1088/0004-637X/737/2/103)
- Scolnic, D., Smith, M., Massiah, A., et al. 2020, *ApJL*, 896, L13, doi: [10.3847/2041-8213/ab8735](https://doi.org/10.3847/2041-8213/ab8735)
- Scolnic, D. M., Jones, D. O., Rest, A., et al. 2018, *ApJ*, 859, 101, doi: [10.3847/1538-4357/aab9bb](https://doi.org/10.3847/1538-4357/aab9bb)
- Shappee, B. J., Holoien, T. W.-S., Drout, M. R., et al. 2019, *ApJ*, 870, 13, doi: [10.3847/1538-4357/aac79](https://doi.org/10.3847/1538-4357/aac79)
- Siebert, M. R., Foley, R. J., Jones, D. O., et al. 2019, *MNRAS*, 486, 5785, doi: [10.1093/mnras/stz1209](https://doi.org/10.1093/mnras/stz1209)
- Slater, C. T., Ivezić, Ž., & Lupton, R. H. 2020, *AJ*, 159, 65, doi: [10.3847/1538-3881/ab6166](https://doi.org/10.3847/1538-3881/ab6166)
- Smith, K. W., Williams, R. D., Young, D. R., et al. 2019, *Research Notes of the American Astronomical Society*, 3, 26, doi: [10.3847/2515-5172/ab020f](https://doi.org/10.3847/2515-5172/ab020f)
- Strateva, I., Ivezić, Ž., Knapp, G. R., et al. 2001, *AJ*, 122, 1861, doi: [10.1086/323301](https://doi.org/10.1086/323301)
- Strolger, L.-G., Dahlen, T., Rodney, S. A., et al. 2015, *ApJ*, 813, 93, doi: [10.1088/0004-637X/813/2/93](https://doi.org/10.1088/0004-637X/813/2/93)
- Suh, H., Yoon, S.-c., Jeong, H., & Yi, S. K. 2011, *ApJ*, 730, 110, doi: [10.1088/0004-637X/730/2/110](https://doi.org/10.1088/0004-637X/730/2/110)
- Sullivan, M., Le Borgne, D., Pritchett, C. J., et al. 2006, *ApJ*, 648, 868, doi: [10.1086/506137](https://doi.org/10.1086/506137)
- Sullivan, M., Conley, A., Howell, D. A., et al. 2010, *MNRAS*, 406, 782, doi: [10.1111/j.1365-2966.2010.16731.x](https://doi.org/10.1111/j.1365-2966.2010.16731.x)
- Tampo, Y., Tanaka, M., Maeda, K., et al. 2020, *ApJ*, 894, 27, doi: [10.3847/1538-4357/ab7ccc](https://doi.org/10.3847/1538-4357/ab7ccc)

- Tonry, J. L., Stubbs, C. W., Lykke, K. R., et al. 2012, ApJ, 750, 99, doi: [10.1088/0004-637X/750/2/99](https://doi.org/10.1088/0004-637X/750/2/99)
- van der Maaten, L., & Hinton, G. 2008, Journal of machine learning research, 9, 2579
- van der Walt, S., Colbert, S. C., & Varoquaux, G. 2011, Computing in Science and Engineering, 13, 22, doi: [10.1109/MCSE.2011.37](https://doi.org/10.1109/MCSE.2011.37)
- van der Wel, A. 2008, ApJL, 675, L13, doi: [10.1086/529432](https://doi.org/10.1086/529432)
- Villar, V. A., Nicholl, M., & Berger, E. 2018, ApJ, 869, 166, doi: [10.3847/1538-4357/aaee6a](https://doi.org/10.3847/1538-4357/aaee6a)
- Virtanen, P., Gommers, R., Oliphant, T. E., et al. 2020, Nature Methods, 17, 261, doi: <https://doi.org/10.1038/s41592-019-0686-2>
- Wang, L., Höflich, P., & Wheeler, J. C. 1997, ApJL, 483, L29, doi: [10.1086/310737](https://doi.org/10.1086/310737)
- Waskom, M., Botvinnik, O., Hobson, P., et al. 2014, seaborn: v0.5.0 (November 2014), v0.5.0, Zenodo, doi: [10.5281/zenodo.12710](https://doi.org/10.5281/zenodo.12710)
- Wiseman, P., Pursiainen, M., Childress, M., et al. 2020, arXiv e-prints, arXiv:2005.08653. <https://arxiv.org/abs/2005.08653>
- York, D. G., Adelman, J., Anderson, John E., J., et al. 2000, AJ, 120, 1579, doi: [10.1086/301513](https://doi.org/10.1086/301513)
- Zhou, L., Liang, Y.-C., Ge, J.-Q., et al. 2019, Research in Astronomy and Astrophysics, 19, 121, doi: [10.1088/1674-4527/19/8/121](https://doi.org/10.1088/1674-4527/19/8/121)